INTERNATIONAL JOURNAL FOR NUMERICAL AND ANALYTICAL METHODS IN GEOMECHANICS
Int. J. Numer. Anal. Meth. Geomech., **22**, 867–901 (1998)

A NUMERICAL PROCEDURE FOR THE ANALYSIS OF THE HYDROMECHANICAL COUPLING IN FRACTURED ROCK MASSES

I. C. DUARTE AZEVEDO[1]*,†, L. E. VAZ[2]‡ AND E. A. VARGAS[2]§

[1] *Civil Engineering Department, Federal University of Viçosa, Minas Gerais, 36571-000 Brazil*
[2] *Civil Engineering Department, Catholic University, Rio de Janeiro, Brazil*

SUMMARY

This work presents a finite element implementation to treat the Hydromechanical Coupling (HM) in fractured rock masses under the framework of the so-called 'equivalent continuum' approach. The multilaminar concept, introduced by Zienkiewicz and Pande,[1] is used to simulate the mechanical behaviour of both the intact rock and the families of fractures. In that concept, the non-linearities in the constitutive relations are dealt by means of fictitious viscoplasticity. In the present implementation, the mechanical behaviour of the fractures is modelled by means of Barton–Bandis model.[2] The shear stress/shear displacement/dilatancy relationship is modelled as viscoplastic and the normal stress/normal displacement as non-linear viscoelastic. Flow along fractures is considered to occur as a sequence of permanent states. The permeability tensor of the equivalent continuum is determined from the hydraulic apertures, in accordance of Barton *et al.*[2] From the numerical point of view, the basic aim of the work is the implementation of an efficient scheme to solve the above described problem. This is done by designing a self-adaptive time step control, transparent to the user, which determines the highest possible time step while assuming the conditions of precision, stability and convergence.[3] The paper presents the numerical details of such scheme together with validation/comparative examples and the results obtained on the analysis of the fractured rock foundation of a hypothetical dam. © 1998 John Wiley & Sons, Ltd.

Key words: finite elements; hydromechanical coupling; fractured rock masses; viscoplasticity

1. INTRODUCTION

The so-called Hydromechanical Coupling (HM) in fractured rock masses has, now for more than two decades, been the subject of considerable experimental and analytical studies. Its relevance in the various engineering works has been pointed out extensively by several authors in slope design, dam foundations, underground excavations, oil recovery, etc.

† Associate Professor
‡ Associate Professor
§ Associate Professor
* Correspondence to: I. C. Duarte Azevedo, Civil Engineering Department, Federal University of Viçosa, Minas Gerais, 36571-000 Brazil

CCC 0363–9061/98/110867–35$17.50

Received 16 January 1997
Revised 17 December 1997

Table I. Implementation of the HM coupling in fractured rock masses

	Fully coupled (in the Biot sense)	Flow as a sequence of permanent states
Discrete block approach	Vargas[5] Lemos and Lorig[6]	Vargas[5] Kafritsas and Einstein[9] Arruda[10]
Joint elements (FE analysis)	Noorishad *et al.*[7]	Wilson[11] Noorishad *et al.*[7]
'Equivalent continuum'	Cho *et al.*[8]	Morgenstern and Guther[12] Erichsen[13] Felipe[14] Present work

In some cases, as in the design of underground structures for nuclear waste repositories, other types of coupling should be considered, with several options of implementation, as shown by Tsang.[4] Despite the fact that the HM coupling was the first amongst the possible relevant coupling phenomena in fractured rock masses to be investigated, studies lack on alternative implementations and on the solution of the numerical problems involved. The HM coupling in fractured rocks can be considered in two ways. In the first, which could be called as fully coupled in the Biot sense, the time changes of volumetric deformations of fractures are taken into account. In the second, flow is considered to take place as a sequence of permanent states, fluid compressibility disregarded. Additionally, the HM coupling has also been treated by considering fractured media as a system of discrete blocks, by using joint elements in standard finite element analysis or as an 'equivalent continuum'. Table I presents these possibilities together with relevant literature. The present work addresses an implementation of the HM coupling as an 'equivalent continuum' under the multilaminar concept[1] with fluid flow taking place as a sequence of permanent states. Barton–Bandis (B–B) model,[2] which incorporates the hydro-mechanical coupling, is the constitutive law adopted for the joints. The shear stress/shear displacement/dilatancy relationship is modelled as viscoplastic and the normal stress/normal displacement as non-linear viscoelastic. The intact rock is considered as a linear and elastic material.

2. QUASI-STATIC ANALYSIS OF THE HM COUPLING UNDER THE MULTILAMINAR CONCEPT

The so-called multilaminar concept was introduced by Zienkiewicz and Pande[1] in order to describe the behaviour of fractured rock masses as an 'equivalent continuum'. The rheological idealization of the multilaminar material is such that non-linearities such as sliding and separation of joints can be incorporated. It presupposes that joints are planar, persistent and parallel. Any number of joint families can be considered.

Zienkiewicz and Pande[1] used a viscoplastic idealization for the rheology of the multilaminar material, as shown in Figure 1. It consists of a spring and viscoplastic units associated in series: the lone spring represents the elastic character of the material and each viscoplastic unit

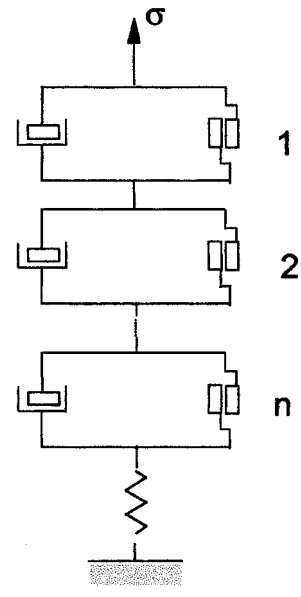

Figure 1. Rheological analogue of multilaminate material

represents one family of joints (an additional unit can be incorporated to represent the visco-plastic behaviour also of the general matrix).

The properties of each viscoplastic unit are described by a yield function, F, and a plastic potential, $Q \cdot F$ and Q are functions of stresses (σ) and the viscoplastic strains (η^{vp}) such that

$$\begin{aligned} F &= F(\sigma, \eta^{\mathrm{vp}}) \\ Q &= Q(\sigma, \eta^{\mathrm{vp}}) \end{aligned} \tag{1}$$

The displacements induced by the application of stresses on the plane of a joint family can be divided into two components: one solely due to changes in normal stresses and another due to changes in normal and tangential stresses,

$$\mathbf{u}_i = \begin{Bmatrix} v \\ u \end{Bmatrix}_i = \begin{Bmatrix} v_{\mathrm{ns}} \\ u_{\mathrm{ss}} \end{Bmatrix}_i + \begin{Bmatrix} v_{\mathrm{nn}} \\ u_{\mathrm{sn}} \end{Bmatrix}_i \tag{2}$$

where the stress vector on a joint family i is given by

$$\sigma_i = \begin{Bmatrix} \sigma_{\mathrm{c}} \\ \tau \end{Bmatrix}_i \tag{3}$$

u is the tangential displacement, v the normal displacement, v_{ns} the normal displacement due to normal and shear stresses (dilatancy), v_{nn} the normal displacement due to normal stress, u_{ss} the tangential displacement due to normal and shear stresses, u_{sn} the tangential displacement due to normal stress (considered equal to zero), σ_{c} the normal stress on joint family and τ the shear stress on joint family.

The deformation of a joint family i, η_i, is defined by the displacement $\mathbf{u}_i$ divided by its spacing s_i

$$\eta_i = \frac{\mathbf{u}_i}{s_i} \tag{4}$$

and

$$\eta_i = \begin{Bmatrix} \eta_v \\ \eta_u \end{Bmatrix}_i = \begin{Bmatrix} \eta_{\mathrm{ns}} \\ \eta_{\mathrm{ss}} \end{Bmatrix}_i + \begin{Bmatrix} \eta_{\mathrm{nn}} \\ \eta_{\mathrm{sn}} = 0 \end{Bmatrix}_i \tag{5}$$

η_u is the tangential strain and η_v the normal strain.

2.1. Viscoplastic modelling of shear behaviour

The rate of viscoplastic strains ($\dot{\eta}^{\mathrm{vp}}$) is given through the concepts of viscoplasticity.[15] The equation that specifies rates of viscoplastic strains, known as flow rule, was proposed by Perzyna[16] and is written for each joint family as

$$\dot{\eta}^{\mathrm{vp}} = \begin{Bmatrix} \dot{\eta}^{\mathrm{vp}}_{\mathrm{ns}} \\ \dot{\eta}^{\mathrm{vp}}_{\mathrm{ss}} \end{Bmatrix}_i = \Phi_i(\sigma, k) \tag{6}$$

$$\Phi_i(\sigma, k) = \bar{\gamma} < \phi(F) > \left(\frac{\partial Q}{\partial \sigma}\right)_i \tag{7a}$$

$$\langle \phi(F) \rangle = \begin{cases} \phi(F) & \text{if } F > 0 \\ 0 & \text{if } F \leqslant 0 \end{cases} \tag{7b}$$

$\bar{\gamma}$ is the fluidity parameter and k the hardening parameter.

The association in series of the rheological analogue, shown in Figure 1, determines that all units are subjected to the same stress and that the total viscoplastic strain rate corresponds to the sum of the viscoplastic strain rates of each individual component. Therefore, the 'equivalent continuum' viscoplastic strain rate vector is given as

$$\dot{\eta}^{\mathrm{vp}} = \sum_{i=1}^{n} \dot{\eta}_i^{\mathrm{vp}} \tag{8}$$

Considering that each joint family may have a different orientation in the rock mass, it is necessary to define a local co-ordinate system for each joint family and a global co-ordinate system for the 'equivalent' continuum, as shown in Figure 2. The matrix which transforms stresses from global to local co-ordinate systems is written, for joint family i, according to Figure 2, as

$$T_{\mathbf{M}_i} = \begin{bmatrix} \sin^2 \beta_i & \cos^2 \beta_i & -2 \sin \beta_i \cos \beta_i \\ -\sin \beta_i \cos \beta_i & \sin \beta_i \cos \beta_i & \cos^2 \beta_i - \sin^2 \beta_i \end{bmatrix} \tag{9}$$

and, therefore,

$$\sigma_i = \mathbf{T}_{\mathbf{M}_i} \sigma \tag{10a}$$

$$\gamma = \mathbf{T}^{\mathrm{T}}_{\mathbf{M}_i} \gamma_i \tag{10b}$$

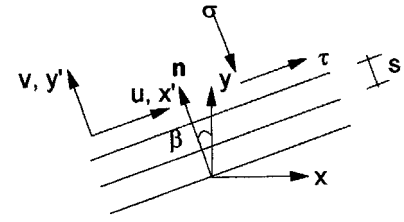

Figure 2. Co-ordinate system in the equivalent continuum

where in plane strain,

$$\gamma_i^{\mathrm{T}} = \{\gamma_v, \gamma_u\} \tag{11a}$$

$$\gamma^{\mathrm{T}} = \{\gamma_x, \gamma_y, \gamma_{xy}\} \tag{11b}$$

$$\sigma^{\mathrm{T}} = \{\sigma_{xx}, \sigma_{yy}, \sigma_{xy}\} \tag{11c}$$

γ_i is the total strain vector of joint family i (local co-ordinate system), γ the total strain vector of 'equivalent continuum' (global co-ordinate system), σ the stress vector (global co-ordinate system) and β_i the angle between local and global co-ordinate axes of joint family i, as shown in Figure 2.

2.2. *Non-linear viscoelastic modelling of normal stress/normal displacement relationship*

Another type of non-linearity present in joint mechanical behaviour refers to the normal stress (σ_c) vs. normal displacement (v_{nn}) relationship. Taking advantage of the fact that viscoplasticity incorporates time as a fictitious independent variable, the non-linear σ_c, vs. v_{nn} relationship is modelled by means of non-linear viscoelasticity. To represent this relationship, Kelvin's model is adopted where the spring parameter is a function of the normal displacement.

The equilibrium of the viscoelastic unit requires that

$$1/\bar{\gamma}\dot{v}_{nn}^{ve} + k_{nn}(v_{nn}^{ve})v_{nn}^{ve} = \sigma_c \tag{12}$$

v_{nn}^{ve} is the viscoelastic normal displacement and k_{nn} the joint secant normal stiffness.

The rheological idealization of the multilaminar material is shown, for the present implementation in Figure 3, where each pair of viscoplastic and viscoelastic units represents one family of joints and the lone spring represents the elastic character of the intact rock. Therefore, for this idealization, the displacements and strains, for a given joint family, induced by normal and shear stresses applied in the plane of the joint, can be written from equations (2) and (4) in the form

$$\mathbf{u}_i = \begin{Bmatrix} v_{ns}^{vp}(\sigma_c, \tau) \\ u_{ss}^{vp}(\sigma_c, \tau) \end{Bmatrix}_i + \begin{Bmatrix} v_{nn}^{ve}(\sigma_c) \\ 0 \end{Bmatrix}_i \tag{13a}$$

$$\eta_i = \begin{Bmatrix} \eta_{ns}^{vp}(\sigma_c, \tau) \\ \eta_{ss}^{vp}(\sigma_c, \tau) \end{Bmatrix}_i + \begin{Bmatrix} \eta_{nn}^{ve}(\sigma_c) \\ 0 \end{Bmatrix}_i \tag{13b}$$

where superscripts vp and ve indicate viscoplastic and viscoelastic, respectively.

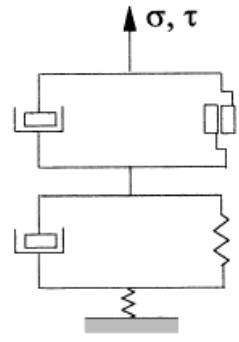

Figure 3. Rheological analogue of fractured rock masses for the viscoplastic–viscoelastic idealization

2.3. Description of B–B joints as viscoplastic/viscoelastic material

To model shear behaviour of B–B joints under the framework of viscoplasticity, in order to establish the constitutive equations, it is necessary that the yield and the potential functions, F and Q, are determined. These functions are not explicit in B–B model[2] but they can be implicitly determined. Expressions (14)–(16) summarize the appropriate functions

$$F = |\tau| - \sigma_c \,\mathrm{tg}\left[\mathrm{JRC}_{\mathrm{mob}} \log\left(\frac{\mathrm{JCS}}{\sigma_c}\right) + \phi_r\right] \tag{14}$$

$$\frac{\partial Q}{\partial \sigma_c} = \mathrm{tg}\left[\frac{1}{M}\mathrm{JRC}_{\mathrm{mob}} \log\left(\frac{\mathrm{JCS}}{\sigma_c}\right)\right] \tag{15}$$

$$\frac{\partial Q}{\partial \tau} = \pm 1 \tag{16}$$

where JRC and JCS are the well-known parameters of B–B model[2], respectively, the joint roughness coefficient and the joint compression strength, and ϕ_r is the joint residual friction angle.[2]

$\mathrm{JRC}_{\mathrm{mob}}$, in the realm of plasticity theory, can be regarded as a hardening parameter and it is related to the shear displacements.[2] M is a user defined damage factor.[2] The terms between brackets in (15) correspond to a dilatancy angle. Expressions (14)–(16) show that B–B model[2] is non-associative in the context of classical plasticity.

To model normal stress–normal displacements for the joints, Barton *et al.*[2] proposed the following relationship:

$$\sigma_c = \frac{k_{ni} V_m}{V_m - v_{nn}} v_{nn} \tag{17}$$

V_m is the joint maximum closure and k_{ni} the joint initial normal stiffness.

Barton *et al.*[2] provide empirical relationships to determine V_m and k_{ni} as function of parameters JRC and JCS.

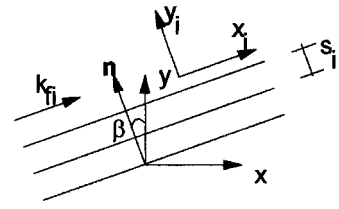

Figure 4. Hydraulic conductivity of joint family i

2.4. Fluid flow

Fluid flow is considered to take place exclusively along joints. Fracture conductivity is a function of the hydraulic aperture. B–B model[2] allows the determination of the hydraulic aperture as function of JRC and the mechanical aperture. As the joint deforms, both mechanical and hydraulic apertures change. The cubic law is assumed valid for flow along fractures and therefore, an equivalent permeability tensor can be determined for each family of persistent joints[17] as

$$\mathbf{k}_{\mathrm{eq}_i} = \frac{e_i}{s_i}\begin{bmatrix} k_{\mathrm{f}_i} & 0 \\ 0 & 0 \end{bmatrix} \tag{18a}$$

$$k_{\mathrm{f}_i} = \frac{g e_i^2}{12\mu} \tag{18b}$$

$\mathbf{k}_{\mathrm{eq}_i}$ is the equivalent permeability tensor of joint family i, e_i the hydraulic aperture of joint family i, k_{f_i} the hydraulic conductivity of joint family i described as planar joint (Figure 4), μ the kinematic viscosity of the fluid and g the gravitational acceleration.

If n families of joints are present in the rock mass, the equivalent permeability tensor, $\mathbf{K}$, for the assemblage of all families is determined as

$$\mathbf{K} = \sum_{i=1}^{n} \mathbf{K}_i \tag{19}$$

where

$$\mathbf{K}_i = \mathbf{T}_{\mathrm{H}_i}^{\mathrm{T}} \mathbf{k}_{\mathrm{eq}_i} \mathbf{T}_{\mathrm{H}_i} \tag{20}$$

is the permeability tensor of joint family i referred to the 'equivalent continuum' co-ordinate system (global system) and

$$\mathbf{T}_{\mathrm{H}_i} = \begin{bmatrix} \cos\beta_i & \sin\beta_i \\ -\sin\beta_i & \cos\beta_i \end{bmatrix} \tag{21}$$

$\mathbf{T}_{H_i}$ is the transformation matrix.

3. A FINITE ELEMENT IMPLEMENTATION OF THE HM COUPLING UNDER THE FRAMEWORK OF VISCOPLASTICITY–VISCOELASTICITY

3.1. Basic equations

3.1.1. Hydraulic model. Fractured rock masses are generally anisotropic and heterogeneous media when represented as an 'equivalent continuum'. In these media, the flow direction is determined by the direction of the joints.

The hydraulic balance, in a steady-state 2-D problem, may be written for an infinitesimal area as

$$\frac{\partial q_x}{\partial x} + \frac{\partial q_y}{\partial y} = \bar{Q} \tag{22}$$

or alternatively

$$\nabla_{\mathrm{H}}^{\mathrm{T}} \mathbf{q} = \bar{Q} \tag{23}$$

$$\mathbf{q} = \begin{Bmatrix} q_x \\ q_y \end{Bmatrix}, \qquad \nabla_{\mathrm{H}}^{\mathrm{T}} = \begin{bmatrix} \dfrac{\partial}{\partial x} & \dfrac{\partial}{\partial y} \end{bmatrix} \tag{24}$$

q_x, q_y is the flow/unit of area of x and y directions, $\bar{Q}$ the specific flow/unit of time, $\mathbf{q}$ the inflow vector and ∇_{H} the operator matrix.

q_x and q_y are related to the hydraulic gradients of the potential function $\phi(x, y)$, as

$$\mathbf{q} = -\mathbf{K} \nabla_{\mathrm{H}} \phi(x, y) \tag{25}$$

$\mathbf{K}$ is the 'equivalent continuum' permeability tensor expressed by equation (19).

Substitution of equation (25) into equation (23) leads to following expression:

$$\nabla_{\mathrm{H}}^{\mathrm{T}} \mathbf{K} \nabla_{\mathrm{H}} \phi(x, y) + \bar{Q} = 0 \tag{26}$$

which represents the hydraulic balance equation, for an infinitesimal area of a 2-D problem, in terms of the potential function.

The boundary conditions associated to a given domain are:

(a) Prescribed potential on the boundary Γ_ϕ

$$\phi(x, y) = \phi_{\mathrm{p}} \tag{27}$$

(b) Prescribed flow on the boundary Γ_q:

$$q_{\mathrm{n}} = q_{\mathrm{p}} \tag{28}$$

where q_{n} is the component of the flow normal to the boundary surface

$$q_{\mathrm{n}} = \mathbf{q}^{\mathrm{T}} \mathbf{n} \tag{29}$$

and $\mathbf{n}$ is the direction cosine vector of an outward normal to the boundary surface,

$$\mathbf{n} = \begin{Bmatrix} n_x \\ n_y \end{Bmatrix} \tag{30}$$

Rearranging terms, the equation representing the boundary condition for a prescribed flow is then obtained as

$$-\{\mathbf{K} \nabla_{\mathrm{H}} \phi(x, y)\}^{\mathrm{T}} \mathbf{n} = q_{\mathrm{p}} \tag{31}$$

3.1.2. Mechanical model. The equilibrium equations for time-dependent 2-D problems in the domain Ω and on the boundary Γ_F are represented, respectively, by

$$\nabla_{\mathrm{M}}^{\mathrm{T}}\dot{\sigma} + \dot{\mathbf{X}} = \mathbf{0} \tag{32}$$

$$\begin{aligned} n_x\dot{\sigma}_{xx} + n_y\dot{\sigma}_{xy} &= \dot{F}_x \\ n_x\dot{\sigma}_{xy} + n_y\dot{\sigma}_{yy} &= \dot{F}_y \end{aligned} \tag{33}$$

where

$$\nabla_{\mathrm{M}}^{\mathrm{T}} = \begin{bmatrix} \dfrac{\partial}{\partial x} & 0 & \dfrac{\partial}{\partial y} \\ 0 & \dfrac{\partial}{\partial y} & \dfrac{\partial}{\partial x} \end{bmatrix} \tag{34}$$

$$\dot{\mathbf{F}}^{\mathrm{T}} = \{\dot{F}_x \;\; \dot{F}_y\} \tag{35a}$$

$$\dot{\mathbf{X}}^{\mathrm{T}} = \{\dot{X}_x \;\; \dot{X}_y\} \tag{35b}$$

$$\dot{\sigma}^{\mathrm{T}} = \{\dot{\sigma}_{xx} \;\; \dot{\sigma}_{yy} \;\; \dot{\sigma}_{xy}\} \tag{35c}$$

∇_{M} is the operator matrix, $\dot{\sigma}$ the stress rate vector, $\dot{\mathbf{X}}$ the body forces rate vector, $\dot{\mathbf{F}}$ the traction forces rate vector.

3.2. Finite element implementation

3.2.1. Hydraulic model. The determination of finite element equations for the hydraulic problem, expressed by equations (26) and (31) follows standard procedures in finite element analysis.[18] The consideration of laminar flow, in a sequence of permanent states, leads to a system of linear equations in finite elements where the unknowns are nodal values of the hydraulic potential

$$\sum_{e=1}^{\mathrm{ne}} \int_{\Omega_e} \mathbf{B}_{\mathrm{H}}^{\mathrm{T}}\mathbf{K}\,\mathbf{B}_{\mathrm{H}}\,\mathrm{d}\Omega_e\,\phi_n = \mathbf{q}_{\mathrm{H}} \tag{36a}$$

$$\mathbf{K}_{\mathrm{H}}\phi_n = \mathbf{q}_{\mathrm{H}} \tag{36b}$$

where

$$\mathbf{K}_{\mathrm{H}} = \sum_{e=1}^{\mathrm{ne}} \int_{\Omega_e} \mathbf{B}_{\mathrm{H}}^{\mathrm{T}}\mathbf{K}\,\mathbf{B}_{\mathrm{H}}\,\mathrm{d}\Omega_e \tag{37}$$

$$\mathbf{q}_{\mathrm{H}} = \sum_{e=1}^{\mathrm{ne}} \left(\int_{\Omega_e} \mathbf{N}_{\mathrm{H}}^{\mathrm{T}}\bar{Q}\,\mathrm{d}\Omega_e + \int_{\Gamma_e} \mathbf{N}_{\mathrm{H}}^{\mathrm{T}} q_p\,\mathrm{d}\Gamma_e \right) \tag{38}$$

$$\mathbf{B}_{\mathrm{H}} = \nabla_{\mathrm{H}}\mathbf{N}_{\mathrm{H}} \tag{39}$$

ne is the number of finite elements, Ω_e the finite element domain, $\mathbf{K}$ the 'equivalent continuum' permeability tensor, Γ_e the element boundary, $\mathbf{B}_{\mathrm{H}}$ the gradient-total head matrix, ϕ_n the vector of

total heads, $\mathbf{q}_H$ the prescribed flow rates and $\mathbf{N}_H$ the matrix of interpolation functions for total heads.

The seepage forces used in the hydromechanical coupling are obtained from the hydraulic gradient vector, **I**, which, in turn, is determined from equation (36b) as

$$\mathbf{I} = -\mathbf{B}_H \phi_n \tag{40}$$

3.2.2. Mechanical model. The same procedure followed for the hydraulic problem is adopted in the finite element formulation of the quasi-static 2-D mechanical problem.[18–21] The principle of virtual displacement allows the derivation of a set of equilibrium equations in rate form as

$$\sum_{e=1}^{ne} \int_{\Omega_e} \mathbf{B}_M^T \dot{\sigma} \, d\Omega_e = \dot{\mathbf{f}}^B + \dot{\mathbf{f}}^\Gamma = \dot{\mathbf{f}}^a \tag{41}$$

$$\dot{\mathbf{f}}^B = \sum_{e=1}^{ne} \int_{\Omega_e} \mathbf{N}_M^T \dot{\mathbf{X}} \, d\Omega_e \tag{42}$$

$$\dot{\mathbf{f}}^\Gamma = \sum_{e=1}^{ne} \int_{\Gamma_e} \mathbf{N}_M^T \dot{\mathbf{F}} \, d\Gamma_e \tag{43}$$

$$\mathbf{B}_M = \nabla_M \mathbf{N}_M \tag{44}$$

$\dot{\mathbf{f}}^B$ is the volumetric force rate vector, $\dot{\mathbf{f}}^\Gamma$ the boundary force rate vector, $\dot{\mathbf{f}}^a$ the total forces applied to the body rate vector, $\mathbf{B}_M$ the strain–displacement matrix and $\mathbf{N}_M$ the matrix of interpolation functions for displacements.

In the present implementation, the initial load method is used to account for the non-linearities of the problem. To describe the inelastic behaviour of the material, the total strain, γ, is decomposed into elastic, ε, and inelastic, η, components, which in rate form writes

$$\dot{\gamma} = \dot{\varepsilon} + \dot{\eta} \tag{45}$$

The elastic strain rate, $\dot{\varepsilon}$, is related to the stress rate, $\dot{\sigma}$, as

$$\dot{\sigma} = \mathbf{D}\dot{\varepsilon} \tag{46}$$

where **D** is the elastic constitutive matrix. The inelastic deformation motion is controlled by a constitutive growth law

$$\dot{\eta} = f(\sigma, \mathbf{p}) \tag{47}$$

where f is a function of stress, σ, and a set of internal variables, **p**. Therefore, the stress–strain relations for the combined material law is given, in rate form, as

$$\dot{\sigma} = \mathbf{D}(\dot{\gamma} - \dot{\eta}) \tag{48}$$

Substituting equation (48) into equation (41) and considering the finite element discretization of the kinematics relations

$$\gamma = \mathbf{B}_M \mathbf{u}_n \tag{49}$$

where $\mathbf{u}_n$ is the nodal displacement vector, the following expression is obtained:

$$\sum_{e=1}^{ne} \int_{\Omega_e} \mathbf{B}_M^T \mathbf{D}(\mathbf{B}_M \dot{\mathbf{u}}_n - \dot{\eta})\, d\Omega_e = \dot{\mathbf{f}}^a \tag{50a}$$

or

$$\mathbf{K}_M \dot{\mathbf{u}}_n - \dot{\mathbf{f}}^{in} = \dot{\mathbf{f}}^a \tag{50b}$$

where

$$\mathbf{K}_M = \sum_{e=1}^{ne} \int_{\Omega_e} \mathbf{B}_M^T \mathbf{D}\, \mathbf{B}_M\, d\Omega_e \tag{51}$$

is the stiffness matrix, and,

$$\dot{f}^{in} = \sum_{e=1}^{ne} \int_{\Omega_e} \mathbf{B}_M^T \mathbf{D}\, \dot{\eta}\, d\Omega_e \tag{52}$$

is the initial load rate vector.

Because of the stress path dependence of the inelastic strain rate, an incremental method of solution is adopted and equations (50) and (52) become

$$\mathbf{K}_M \Delta \mathbf{u}_n = \Delta \mathbf{f}^a + \Delta \mathbf{f}^{in} \tag{53}$$

$$\Delta \mathbf{f}^{in} = \sum_{e=1}^{ne} \int_{\Omega_e} \mathbf{B}_M^T \mathbf{D}\, \Delta\eta\, d\Omega_e \tag{54}$$

which corresponds to a discretization in time of the stress–strain relation for the combined material

$$\Delta\sigma = \mathbf{D}(\Delta\gamma - \Delta\eta) \tag{55}$$

where

$$\Delta\eta = \int_{t_n}^{t_{n+1}} \dot{\eta}\, dt \tag{56}$$

has to be evaluated numerically within the time step. In order to control the numerical properties, such as stability of the integration process and convergence of the iterative solution, appropriate values of time interval have to be established. The determination of critical time steps is shown in section 4.

3.2.3. Hydromechanical coupling. The inelastic process marches on time according to equation (52). At the end of each time increment, hydraulic apertures are corrected and flow analysis takes place producing seepage forces at each Gauss integration point of the finite elements. These forces, obtained from the hydraulic problem, may be calculated, in an incremental form as

$$\Delta \mathbf{f}^p = \sum_{e=1}^{ne} \int_{\Omega_e} \mathbf{N}_H^T \gamma_w \mathbf{I}\, d\Omega_e \tag{57}$$

γ_w is the water specific weight, **I** the hydraulic gradient (equation 40) and $\Delta \mathbf{f}^p$ the increment of seepage force vector.

The integration of these forces in the element gives equivalent nodal forces for the mechanical analysis in the following time step. The increment of seepage forces is added to the increments of applied body and boundary forces of the mechanical problem, Δf^a, and to the increment of inelastic pseudo-forces, Δf^{in}, leading to the following set of equilibrium equations:

$$\mathbf{K}_M \Delta \mathbf{u}_n = \Delta \mathbf{f}^a + \Delta \mathbf{f}^{in} + \Delta \mathbf{f}^p \tag{58}$$

In each time increment, equation (58) must be solved iteratively since $\Delta \mathbf{f}^{in}$, due to the non-linearities in the constitutive law, is not known *a priori*.

As the hydromechanical coupling is simulated as a sequence of permanent states, the effect of seepage is taken into account with the correction of the seepage forces at the end of each time level.

The process marches in time until convergence is eventually obtained. The convergence condition for the coupled problem must be monitored at two levels:

(1) In the mechanical problem, convergence is assumed when the process reaches a steady-state condition (as pointed out before, the rate dependence is only a mathematical artifice for the solution of the non-linear constitutive equations through the initial load method). Stationary conditions are controlled, at the end of each time increment, by the ratio of the sum of rates of effective inelastic deformations, at all Gauss integration points of the current time step, and the rates in the first time increment:

$$\frac{\sum_{m=1}^{NG} (\dot{\eta}_{ef_m})_t}{\sum_{m=1}^{NG} (\dot{\eta}_{ef_m})_1} \leqslant \mathrm{TOL} \tag{59}$$

NG is the number of Gauss points, $\dot{\eta}_{ef}$ the total effective inelastic strain rate in a Gauss point[15] and TOL the tolerance for convergence.

$$\Delta \eta_{ef} = \sqrt{2/3}\, \|\Delta \eta\| \tag{60}$$

$$\dot{\eta}_{ef} = \frac{\Delta \eta_{ef}}{\Delta t} \quad \text{(in each Gauss point)} \tag{61}$$

Inside each time step, the iterative process is checked by the norm

$$\frac{\|\Delta \eta^{i+1}\| - \|\eta^i\|}{\|\Delta \eta^{i+1}\|} \leqslant \mathrm{TOL1} \tag{62}$$

$\Delta \eta^{i+1}$ is the inelastic strain increment vector at a Gauss point in iteration $i+1$, $\Delta \eta^i$ the inelastic strain increment vector at a Gauss point in iteration i and TOL1 the tolerance for convergence.

(2) Convergence of the hydraulic problem, monitored by the norm expressed by equation (63), is assumed when the increment of seepage forces is negligible, that is,

$$\frac{\sum_{i=1}^{N} (\Delta f_i^p)^t - \sum_{i=1}^{N} (\Delta f_i^p)^{t-\Delta t}}{\sum_{i=1}^{N} (\Delta f_i^p)^1} \leqslant \mathrm{TOL2} \tag{63}$$

N is the number of nodes, $(\Delta f_i^p)^t$ the increment of seepage force at node i at instant t, $(\Delta f_i^p)^{t-\Delta t}$ the increment of seepage force at node i at instant $(t-\Delta t)$, $(\Delta f_i^p)^1$ the increment of seepage force at node i at instant 1 and TOL2 the tolerance for convergence.

4. A PROPOSAL FOR A SELF-ADAPTIVE TIME-STEP CONTROL

4.1. Polynomial approximation

In order to determine the pseudo-forces vector, Δf^i, expressed by equation (54), the increment of inelastic strains, $\Delta\eta$, must be estimated. Since the mechanical problem is considered as time-dependent, the inelastic strain vector, η, is represented as a polynomial function of the time variable, t, within the time interval, Δt. Linear and cubic approximations may be used to represent the variation of η in Δt. At an instant ζ of Δt, where ζ represents the weighting strategy for computing the inelastic strain increment, a linear approximation of η may be represented by

$$\eta_\zeta = (1-\zeta)\eta_n + \zeta\eta_{n+1} \tag{64}$$

$$\dot{\eta}_\zeta = \frac{\mathbf{1}}{\Delta t}(\eta_{n+1} - \eta_n) \tag{65a}$$

$$\zeta = \frac{t_\zeta}{\Delta t} \tag{65b}$$

η_ζ is the inelastic strain vector at an instant ζ of time interval Δt, η_n the inelastic strain vector at the beginning of time interval, t_n, η_{n+1} the inelastic strain vector at the end of time interval, t_{n+1} and t_ζ the instant ζ of time interval Δt.

Accuracy can be improved by using higher-order time expansions of η within each time step. The cubic Hermitean algorithm supposes known values of the state variables and its derivatives at the beginning and at the end of the time interval but has as an advantage of the possibility of eliminating these derivatives through the differential statement. Therefore, for the cubic interpolation in Δt, the expression for the inelastic strain may be written as

$$\eta_\zeta = w_0\eta_n + \Delta t\,\bar{w}_0\dot{\eta}_n + w_1\eta_{n+1} + \Delta t\,\bar{w}_1\dot{\eta}_{n+1} \tag{66}$$

$\dot{\eta}_n$ is the inelastic strain rate vector at the beginning of time interval, t_n and $\dot{\eta}_{n+1}$ the inelastic strain rate vector at the end of time interval, t_{n+1}.

Time derivatives of η_ζ yields

$$\dot{\eta}_\zeta = \frac{\mathbf{1}}{\Delta t}\{w_0'\eta_n + \Delta t\,\bar{w}_0'\dot{\eta}_n + w_1'\eta_{n+1} + \Delta t\,\bar{w}_1'\dot{\eta}_{n+1}\} \tag{67}$$

$$\begin{aligned} w_0 &= 1 - 3\zeta^2 + 2\zeta^3, & w_1 &= 3\zeta^2 - 2\zeta^3 \\ \bar{w}_0 &= \zeta - 2\zeta^2 + \zeta^3, & \bar{w}_1 &= -\zeta^2 + \zeta^3 \\ w_0' &= -6\zeta + 6\zeta^2\ , & w_1' &= 6\zeta - 6\zeta^2 \\ \bar{w}_0' &= 1 - 4\zeta + 3\zeta^2, & \bar{w}_1' &= -2\zeta + 3\zeta^2 \end{aligned} \tag{68}$$

Particular values ζ such as 0, $\frac{1}{2}$, $\frac{2}{3}$ and 1, correspond to special time levels in the time interval Δt yielding the well-known forward, trapezoidal, Galerkin and backward algorithms, respectively.

4.2. Properties of the algorithms

For a good computational efficiency, it is necessary that the algorithm fulfils requirements of precision, stability and convergence.

The precision of the algorithm is determined by comparing the terms in Taylor series expansion of the solution function with the terms of the Taylor series expansion of the approximate function. The first terms, which differ in the two series, represent the truncation error. Truncation error is unavoidable. However, it can be made as small as possible by using better approximate functions.

Stability of the time step integration is assured if the numerical solution is not significantly distorted by round-off errors in the time marching process. A method is said to be stable if the amplification function, which relates the solutions at the end and at the beginning of the time interval, satisfies the local stability constraint. In the one-dimensional case, this property may be represented as

$$\left| \frac{\mathrm{d}\eta_{n+1}}{\mathrm{d}\eta_n} \right| \leqslant 1 \tag{69}$$

$\mathrm{d}\eta_n$ is the increment of inelastic strain at the beginning of time interval, t_n, and $\mathrm{d}\eta_{n+1}$ the increment of inelastic strain at the end of time interval, t_{n+1}.

The sufficient condition for convergence of an iterative process is that the difference between two successive increments of the state variable, $\mathrm{d}\eta^i$ and $\mathrm{d}\eta^{i+1}$, becomes smaller approaching zero when i goes to infinity. That is,

$$\left| \frac{\mathrm{d}\eta^{i+1}}{\mathrm{d}\eta^i} \right| < 1 \tag{70}$$

In what follows, it is admitted that time-step requirements for stability and convergence for the non-linear viscoelastic and viscoplastic processes are independently evaluated. In so doing, the lesser of the two will be adopted.

4.3. Algorithms for the viscoplastic analysis

The viscoplastic rate law, given by equation (6), is readily discretized by expanding the viscoplastic strain, η^{vp}, into a piecewise linear polynomial between the nodal values, η_n^{vp} and η_{n+1}^{vp}. Interpolation in the normalized time variable $0 \leqslant \zeta \leqslant 1$ yields, for each joint family, according to equation (64)

$$\eta_{\zeta_i}^{\mathrm{vp}} = (1 - \zeta)\eta_{n_i}^{\mathrm{vp}} + \zeta\eta_{n+1_i}^{\mathrm{vp}} \tag{71}$$

In the estimate of critical time steps, however, the hardening parameter, k, in equation (6), is admitted, for simplicity, to be constant in each time step and thus, the viscoplastic strain

increment is given as

$$\Delta\eta_i^{\mathrm{vp}} = (\eta_{n+1}^{\mathrm{vp}} - \eta_n^{\mathrm{vp}}) = (\Delta t\dot{\eta}^{\mathrm{vp}})_i = \Delta t\Phi(\sigma_\zeta)_i \tag{72}$$

where σ_ζ is the stress vector at an instant ζ of time interval, Δt

$$\sigma_\zeta^{\mathrm{T}} = \{\sigma_\zeta \quad \tau_\zeta\}_i \tag{73a}$$

and

$$\Delta\eta_i^{\mathrm{vp}^{\mathrm{T}}} = \{\Delta\eta_v^{\mathrm{vp}} \ \ \Delta\eta_u^{\mathrm{vp}}\}_i \tag{73b}$$

Therefore, with the inclusion of the elastic component representing the intact rock, the following algebraic form of the constitutive rate law (equation (48)) is now written for the 'equivalent material' as

$$\Delta\sigma = \mathbf{D}(\Delta\gamma - \Delta\eta^{\mathrm{vp}}) \tag{74a}$$

or

$$\sigma_{n+1} = \sigma_n + \mathbf{D}\Delta\gamma - \mathbf{D}\Delta\eta^{\mathrm{vp}} \tag{74b}$$

where from equation (8)

$$\Delta\eta^{\mathrm{vp}} = \sum_{i=1}^{n} \Delta\eta_i^{\mathrm{vp}} \tag{75}$$

According to equation (71), the finite time expansion of the viscoplastic strain is implicit and some interaction between the total strain increment, $\Delta\gamma$, which appears as a driving force on the right-hand side of equation (74b) in place of the structural response, has to be considered.[22] Therefore, in order to examine the numerical solution of the constitutive growth law, Argyris *et al.*,[22] characterize the structural response to inelastic excitations by the 'structural dissipation parameter', β,

$$\beta = \frac{\partial\gamma}{\partial\eta} = \begin{cases} \mathbf{0} & \text{if } \mathrm{d}\gamma = 0 \\ \mathbf{I} & \text{if } \mathrm{d}\sigma = \mathbf{0} \end{cases} \tag{76}$$

which varies between $\mathbf{0} \leqslant \beta \leqslant \mathbf{I}$, where $\mathbf{I}$ is the identity matrix, depending on the extent of stress or strain control. In the limiting case of pure creep, with $\mathrm{d}\sigma = \mathbf{0}$, the inelastic strain rate, $\mathrm{d}\eta$, converts entirely into the total strain rate $\mathrm{d}\gamma$. On the other hand, for pure relaxation, with $\mathrm{d}\gamma = 0$, the inelastic strain rate causes a corresponding reduction of stress $\mathrm{d}\sigma = -\mathbf{D}\,\mathrm{d}\eta$.

As pointed out in the previous item, stability can be accessed by examining the matrix, which relates the increment of the state variables at the end and at the beginning of the time interval. Assuming $\Delta\gamma$ being prescribed, which corresponds to the worst situation for amplification of stresses,[22] the differentiation of equation (74b) gives the following expression between the differential stresses at subsequent instants of time:

$$\mathrm{d}\sigma_{n+1} = \mathbf{d}\sigma_n - \mathbf{D}\left(\frac{\partial\Delta\eta^{\mathrm{vp}}}{\partial\sigma_n}\,\mathrm{d}\sigma_n + \frac{\partial\Delta\eta^{\mathrm{vp}}}{\partial\sigma_{n+1}}\,\mathrm{d}\sigma_{n+1}\right) \tag{77a}$$

or,

$$\mathrm{d}\sigma_{n+1} = \left(\mathbf{I} + \mathbf{D}\frac{\partial\Delta\eta^{\mathrm{vp}}}{\partial\sigma_{n+1}}\right)^{-1}\left[\mathbf{I} - \mathbf{D}\frac{\partial\Delta\eta^{\mathrm{vp}}}{\partial\sigma_n}\right]\mathrm{d}\sigma_n \tag{77b}$$

From the chain rule,

$$\frac{\partial \Delta \eta^{\mathrm{vp}}}{\partial \sigma_{n+1}} = \frac{\partial \Delta \eta^{\mathrm{vp}}}{\partial \sigma_{\zeta}} \frac{\partial \sigma_{\zeta}}{\partial \sigma_{n+1}} \tag{78a}$$

$$\frac{\partial \Delta \eta^{\mathrm{vp}}}{\partial \sigma_{n}} = \frac{\partial \Delta \eta^{\mathrm{vp}}}{\partial \sigma_{\zeta}} \frac{\partial \sigma_{\zeta}}{\partial \sigma_{n}} \tag{78b}$$

and considering a linear expansion of the stress vector, σ_{ζ}

$$\sigma_{\zeta} = (1 - \zeta)\sigma_{n} + \zeta \sigma_{n+1} \tag{79}$$

equation (78) may be written as

$$\frac{\partial \Delta \eta^{\mathrm{vp}}}{\partial \sigma_{n+1}} = \frac{\partial \Delta \eta^{\mathrm{vp}}}{\partial \sigma_{\zeta}} \zeta \tag{80a}$$

$$\frac{\partial \Delta \eta^{\mathrm{vp}}}{\partial \sigma_{n}} = \frac{\partial \Delta \eta^{\mathrm{vp}}}{\partial \sigma_{\zeta}} (1 - \zeta) \tag{80b}$$

or, taking into consideration equation (72)

$$\frac{\partial \Delta \eta^{\mathrm{vp}}}{\partial \sigma_{n+1}} = \mathbf{G}_{\zeta} \zeta \Delta t \tag{81a}$$

$$\frac{\partial \Delta \eta^{\mathrm{vp}}}{\partial \sigma_{n}} = \mathbf{G}_{\zeta} (\mathbf{1} - \zeta) \Delta t \tag{81b}$$

Matrix $\mathbf{G}_{\zeta}$ may be written as

$$\mathbf{G}_{\zeta} = \sum_{i=1}^{nf} \left[\left(\frac{\partial \Phi(\sigma)}{\partial \sigma} \right)_{i} \right]_{\zeta} \tag{82a}$$

or

$$\mathbf{G}_{\zeta} = \sum_{i=1}^{nf} (\mathbf{T}_{\mathbf{M}_i}^{\mathrm{T}} \psi_{i_{\zeta}} \mathbf{T}_{\mathbf{M}_i}) \tag{82b}$$

where

$$\psi_{i_{\zeta}} = \begin{bmatrix} \dfrac{\partial \Phi_1}{\partial \sigma_{\mathbf{c}_{\zeta}}} & \dfrac{\partial \Phi_1}{\partial \tau_{\zeta}} \\ \dfrac{\partial \Phi_2}{\partial \sigma_{\mathbf{c}_{\zeta}}} & \dfrac{\partial \Phi_2}{\partial \tau_{\zeta}} \end{bmatrix} \tag{83a}$$

and from equation (7a)

$$\Phi_i = \begin{Bmatrix} \Phi_1 \\ \Phi_2 \end{Bmatrix}_i = \begin{Bmatrix} \bar{\gamma} < \phi(F) > \dfrac{\partial Q}{\partial \sigma_{c_{\zeta}}} \\ \bar{\gamma} < \phi(F) > \dfrac{\partial Q}{\partial \tau_{\zeta}} \end{Bmatrix}_i \tag{83b}$$

Substitution of equations (81) into equation (77b) yields

$$\mathrm{d}\sigma_{n+1} = [\mathbf{I} + \mathbf{D}\mathbf{G}_\zeta \zeta \Delta t]^{-1}[\mathbf{I} - \mathbf{D}\mathbf{G}_\zeta (1-\zeta)\Delta t]\,\mathrm{d}\sigma_n \tag{84a}$$

$$\mathrm{d}\sigma_{n+1} = \mathbf{R}^\zeta \mathrm{d}\sigma_n \tag{84b}$$

where the amplification matrix, $\mathbf{R}^\zeta$, is given as

$$\mathbf{R}^\zeta = \frac{[\mathbf{I} - \mathbf{D}\mathbf{G}_\zeta (1-\zeta)\Delta t]}{[I + \mathbf{D}\mathbf{G}_\zeta \zeta \Delta t]} \tag{85}$$

The local stability condition is satisfied if

$$\|\mathbf{R}^\zeta\| \leqslant 1 \tag{86}$$

Thus, the critical stability time step, $\Delta t_{\mathrm{s}}^{\mathrm{vp}}$, can be calculated from equation (86) as

$$\Delta t_{\mathrm{s}}^{\mathrm{vp}} = \frac{2}{(1-2\zeta)\rho_\zeta} \tag{87}$$

where ρ_ζ is the spectral radius (maximum eigenvalue) of matrix $\mathbf{D}\mathbf{G}_\zeta$. For values of $\zeta \geqslant 1/2$ unconditional stability is guaranteed.

The convergence behaviour of the iterative process may be accessed by examining the incremental stress-strain relation at the constitutive level,

$$\sigma_{n+1}^{i+1} = \sigma_n + \mathbf{D}(\gamma_{n+1}^i - \gamma_n) - \mathbf{D}(\eta_{n+1}^{\mathrm{vp}^i} - \eta_n^{\mathrm{vp}}) \tag{88}$$

where superscripts i and $i+1$ refer to two consecutive iterations. Differentiation of equation (88) yields

$$\mathrm{d}\sigma_{n+1}^{i+1} = \mathbf{D}\left(\frac{\partial \gamma_{n+1}}{\partial \eta_{n+1}^{\mathrm{vp}}} \frac{\partial \eta_{n+1}^{\mathrm{vp}}}{\partial \sigma_{n+1}} \frac{\partial \eta_{n+1}^{\mathrm{vp}}}{\partial \sigma_{n+1}}\right) \mathrm{d}\sigma_{n+1}^i \tag{89}$$

From the chain rule, in analogy to equation (78), considering a linear interpolation of the stress vector, σ_ζ, defined by equation (79) and introducing equations (76) and (81), equation (87) becomes

$$\mathrm{d}\sigma_{n+1}^{i+1} = \mathbf{D}(\beta - \mathbf{I})\zeta \Delta t \mathbf{G}_\zeta \,\mathrm{d}\sigma_{n+1}^i \tag{90a}$$

$$\mathrm{d}\sigma_{n+1}^{i+1} = \mathbf{C}^\zeta \mathrm{d}\sigma_{n+1}^i \tag{90b}$$

where

$$\mathbf{C}^\zeta = \mathbf{D}(\beta - \mathbf{I})\zeta \Delta t \mathbf{G}_\zeta \tag{91}$$

Convergence of the iterative process is then assured if

$$\|\mathbf{C}^\zeta\| < 1 \tag{92}$$

Considering the most critical situation of non-structural dissipation,[22] $\beta = \mathbf{0}$, the convergence critical time step, $\Delta t_{\mathrm{c}}^{\mathrm{vp}}$, is defined from equation (92) as

$$\Delta t_{\mathrm{c}}^{\mathrm{vp}} = \frac{1}{\zeta \rho_\zeta} \tag{93}$$

The coefficients of matrix ψ_{i_ζ} (equation (83a)) for B–B constitutive model are given in the appendix and may be used to calculate the spectral radius, ρ_ζ, in the estimate of critical stability and convergence time steps for this model.

4.4. Algorithms for the viscoelastic analysis

The constitutive relation for each joint family represented by this model is expressed, in terms of strains, from equation (12), through,

$$(\dot{\eta}^{\mathrm{ve}} + \lambda \eta^{\mathrm{ve}} = \bar{\gamma}\sigma_{\mathrm{c}})_i \tag{94}$$

$$\lambda_i = \bar{\gamma} k(\eta^{\mathrm{ve}})_i \tag{95}$$

$k(\eta^{\mathrm{ve}})_i$ is the non-linear secant normal stiffness of joint family i.

For simplicity, the subscript i, which refers to a specific family of joints, will be omitted in the equations that follow.

Considering linear expansions of η^{ve} and of $\sigma_{\mathrm{c}_\zeta}$ (equations (94a) and (95)), in a normalized time interval, similarly to what was done for the viscoplastic problem

$$\eta^{\mathrm{ve}}_\zeta = (1-\zeta)\eta^{\mathrm{ve}}_n + \zeta \eta^{\mathrm{ve}}_{n+1} \tag{96a}$$

$$\Delta\eta^{\mathrm{ve}} = \dot{\eta}^{\mathrm{ve}}_\zeta \Delta t \tag{96b}$$

$$\sigma_{\mathrm{c}_\zeta} = (1-\zeta)\sigma_{\mathrm{c}_n} + \zeta \sigma_{\mathrm{c}_{n+1}} \tag{97}$$

and substituting the resulting expressions, equations (96a) and (97) into equation (94), the viscoelastic strain at an instant t_ζ of the time interval can be written as

$$\eta^{\mathrm{ve}}_{n+1} = \frac{1-(1-\zeta)\lambda_\xi \Delta t}{1+\zeta\lambda_\zeta \Delta t}\,\eta^{\mathrm{ve}}_n + \frac{\bar{\gamma}\Delta t}{1+\zeta\lambda_\zeta\Delta t}\,\sigma_{\mathrm{c}_\zeta} \tag{98a}$$

or

$$\eta^{\mathrm{ve}}_{n+1} = R^\zeta \eta^{\mathrm{ve}}_n + H^\zeta \sigma_{\mathrm{c}_\zeta} \tag{98b}$$

$$R^\zeta = \frac{1-(1-\zeta)\lambda_\zeta \Delta t}{1+\zeta\lambda_\zeta\Delta t} \tag{99a}$$

$$H^\zeta = \frac{\bar{\gamma}\Delta t}{1+\zeta\lambda_\zeta\Delta t} \tag{99b}$$

Comparing the Taylor series expansion of the analytical solution of equation (94) with the polynomial expansion correspondent to the approximate solution given by equation (98), it can be shown[22] that the most accurate algorithm corresponds to the particular value of $\zeta = 1/2$. The property of accuracy is valid, however, in the neighbourhood of $\Delta t = 0$. A reasonable value for a precise approximation would then be $\lambda_\zeta \Delta t < 1$. That is,

$$\Delta t^{\mathrm{ve}}_{\mathrm{a}} = \frac{1}{\lambda_\zeta} \tag{100}$$

where $\Delta t^{\mathrm{ve}}_{\mathrm{a}}$ is the critical time step for accuracy.

Stability is guaranteed, in this case, if,

$$\|R^{\zeta}\| \leqslant 1 \tag{101}$$

Therefore, the critical stability time step to satisfy equation (101) is determined as

$$\Delta t_{\mathrm{s}}^{\mathrm{ve}} = \frac{2}{(1-2\zeta)\lambda_{\zeta}} \tag{102}$$

Again, for values of $\zeta \geqslant 1/2$, unconditional stability is assured.

An oscillatory behaviour is present when $-1 < R^{\zeta} < 0$. The backward algorithm ($\zeta = 1$) is the only one that is free from such behaviour, for arbitrary ζ-values. This kind of behaviour will be also present in Crank–Nicholson ($\zeta = 1/2$) and in Galerkin ($\zeta = 2/3$) algorithms, whenever Δt equals $2/\lambda_{\zeta}$ and $3/\lambda_{\zeta}$, respectively.

The analysis of convergence of the algorithm for the viscoelastic analysis, and the subsequent determination of a critical convergence time step, starts with the differentiation of equation (98) which gives, for the non-linear case, when λ is a function of η^{ve}, the following expression:

$$\mathrm{d}\eta_{n+1}^{\mathrm{ve}^{i+1}} = \mathrm{d}R^{\zeta}(\eta_{\zeta}^{\mathrm{ve}})\eta_{n}^{\mathrm{ve}^{i}} + R^{\zeta}(\eta_{\zeta}^{\mathrm{ve}})\mathrm{d}\eta_{n}^{\mathrm{ve}^{i}} + \mathrm{d}H^{\zeta}(\eta_{\zeta}^{\mathrm{ve}})\sigma_{\mathrm{c}_{\zeta}}^{i} + H^{\zeta}(\eta_{\zeta}^{\mathrm{ve}})\,\mathrm{d}\sigma_{\mathrm{c}_{\zeta}}^{i} \tag{103}$$

From the chain rule

$$\mathrm{d}R^{\zeta} = \frac{\partial R^{\zeta}}{\partial \eta_{\zeta}^{\mathrm{ve}}}\frac{\partial \eta_{\zeta}^{\mathrm{ve}}}{\partial \eta_{n+1}^{\mathrm{ve}}}\,\mathrm{d}\eta_{n+1}^{\mathrm{ve}^{i}} \tag{104a}$$

$$\mathrm{d}H^{\zeta} = \frac{\partial H^{\zeta}}{\partial \eta_{\zeta}^{\mathrm{ve}}}\frac{\partial \eta_{\zeta}^{\mathrm{ve}}}{\partial \eta_{n+1}^{\mathrm{ve}}}\,\mathrm{d}\eta_{n+1}^{\mathrm{ve}^{i}} \tag{104b}$$

$$\mathrm{d}\sigma_{\mathrm{c}_{\zeta}}^{i} = \frac{\partial \sigma_{\mathrm{c}_{\zeta}}}{\partial \eta_{\zeta}^{\mathrm{ve}}}\frac{\partial \eta_{\zeta}^{\mathrm{ve}}}{\partial \eta_{n+1}^{\mathrm{ve}}}\,\mathrm{d}\eta_{n+1}^{\mathrm{ve}^{i}} \tag{104c}$$

and according to Argyris *et al.*,[22]

$$\frac{\partial \sigma_{\mathrm{c}_{\zeta}}}{\partial \eta_{\zeta}^{\mathrm{ve}}} = E_{\mathrm{r}}(\beta - 1) \tag{104d}$$

Substituting equations (17), (99) and (104) into equation (103) yields

$$\mathrm{d}\eta_{n+1}^{\mathrm{ve}^{i+1}} = P^{\zeta}\,\mathrm{d}\eta_{n}^{\mathrm{ve}^{i}} \tag{105}$$

where

$$P^{\zeta} = \frac{-\bar{\gamma}\Delta t\, k_{ni} V_{\mathrm{m}} \zeta(\eta_{n}^{\mathrm{ve}} + \bar{\gamma}\Delta t\zeta\sigma_{\mathrm{c}_{\zeta}})}{(V_{\mathrm{m}}/s - \eta_{\zeta}^{\mathrm{ve}})^2(1+\zeta\lambda_{\zeta}\Delta t)^2} + \frac{\bar{\gamma}\Delta t E_{\mathrm{r}}(\beta-1)\zeta}{(1+\zeta\lambda_{\zeta}\Delta t)} \tag{106}$$

and E_{r} is the Young modulus of the intact rock.

Imposing the convergence condition to P^{ζ} defined above, and considering the structural dissipation parameter, β, equal to zero,[22] the convergence time interval is obtained from a second

degree expression given by

$$A\Delta t^2 + B\Delta t + C > 0 \tag{107}$$

$$A = -\bar{\gamma}^2\zeta^2 k_{ni} V_{\mathrm{m}} \sigma_{\mathrm{c}_\zeta} + (V_{\mathrm{m}}/s - \eta_\zeta^{\mathrm{ve}})^2 \zeta^2 \lambda_\zeta (\lambda_\zeta - \bar{\gamma} E_{\mathrm{r}})$$

$$B = (V_{\mathrm{m}}/s - \eta_\zeta^{\mathrm{ve}})^2 \zeta (2\lambda_\zeta - \bar{\gamma} E_{\mathrm{r}}) - \bar{\gamma}\zeta k_{ni} V_{\mathrm{m}} \eta_n^{\mathrm{ve}} \tag{108}$$

$$C = (V_{\mathrm{m}}/s - \eta_\zeta^{\mathrm{ve}})^2$$

The time step that should be adopted for the solution of a real problem in a fractured rock mass is the minimum among all the critical values determined for convergence, stability and accuracy of the viscoplastic and viscoelastic solutions (critical time intervals for the cubic interpolation in Δt, in the case of a single joint, are presented in Duarte[3]).

Critical time step lengths for a number of yield criteria have already been proposed by Cormeau.[23] However, Cormeau[23] considered only models for perfect elastoplastic continua, as the classical Von Mises, Drucker–Prager, Tresca and Mohr–Coulomb criteria. Besides, his results are only valid for a homogeneous continuous medium.

5. DEVELOPED CODE

A finite element program (VISCO1), written in FORTRAN77, was developed.[25,14,3] This code allows a bidimensional analysis, linear and non-linear, of the mechanical and hydromechanical behaviour (coupled and uncoupled) of continuous and fractured rock masses. The finite element used is the eight-node isoparametric element of the Serendipity family.

The expressions of time increments presented above, equations (87), (93), (100), (102) and (107), are implemented in the program and critical time steps are automatically calculated. More specifically, at each time step the program calculates—at each Gauss integration point of all elements in the mesh—the values of Δt, regarding convergence, stability and precision (only for the viscoelastic analysis) of the numerical process, for each of the two idealizations considered, viscoplastic and viscoelastic (for this idealization, for each family of joints). The critical time step will be the smallest one found and will be used for the whole structure. As this value is implicitly calculated, it is corrected (or adapted) at each step, generating a self-adaptive time step process.

6. EXAMPLES

In order to validate and demonstrate the adequacy of the expressions obtained for critical time step increments, three examples are presented.

These examples have already been presented in other publications[25, 14, 26] where there was no control of the time increments used in the time integration process, that is, these values had to be arbitrarily chosen and convergence could not be always guaranteed. The objective of the examples presented here is to illustrate the efficiency of an automatic and auto-adaptive definition of adequate integration time steps.

Being unconditionally stable and presenting a better accuracy compared to the other algorithms mentioned in Section 4.4, the Crank–Nicholson algorithm ($\zeta = 1/2$) is used in the examples.

6.1. Example 1. Relative displacements of a joint family due to an applied (σ_c, τ) *loading*

In this example, normal, shear and dilatant displacements of a single joint family, subjected to various loading (normal, σ_c, and shear, τ) conditions are calculated through program VISCO1. Figure 5 shows the problem represented as an equivalent continuum and Figure 6 presents the adopted finite element discretization. Intact rock and joint properties are presented below:

Intact rock properties		Joint properties	
E_r	10^5 MPa	JRC	16·6
ν_r	0·0	JCS	30 MPa
		ϕ_r	32°
		a_j	0·0002 m
		LN	0·1 m
		s	1·0 m

Table II presents the analytical and the numerical results of normal and shear displacements of the joint family described by Barton–Bandis[2] elastoplastic model. The correspondence between

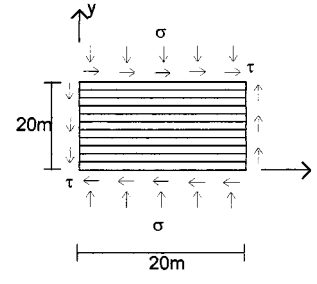

Figure 5. Joint family as part of an equivalent continuum

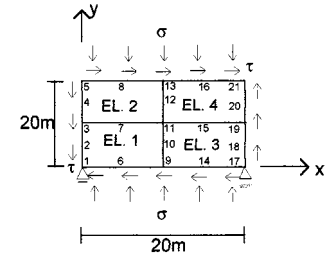

Figure 6. Finite element mesh

Table II. Normal (v) and shear (u) displacements for a single joint family with auto-adaptive and with arbitrarily prescribed time steps (Δt) (u and $v \times 10^{-4}$) m

		Analyt.		Auto-adaptive Δt TOL=TOL1=10^{-2}			Auto-adaptive Δt TOL=TOL1=10^{-3}			$\Delta t = 0{\cdot}01$			$\Delta t = 0{\cdot}1$		
σ_c	τ	u	v	u	v	NS	u	v	NS	u	v	NS	u	v	NS
0·3	0·1	1·73	−0·11	1·68	−0·11	756	1·72	−0·11	1030	1·71	−0·11	80	1·73	−0·11	13
0·5	0·3	2·90	−0·18	2·86	−0·18	309	2·90	−0·18	444	2·89	−0·18	45	2·90	−0·18	10
1·0	0·1	0·54	−0·33	0·49	−0·33	179	0·53	−0·33	325	0·53	−0·33	22	0·48	−0·33	19
5·0	4·0	5·06	−0·82	4·95	−0·84	83	5·05	−0·82	126	5·03	−0·95	12	D	D	D
10·0	1·0	0·54	−1·57	0·49	−1·57	50	0·53	−1·57	88	0·53	−1·57	8	D	D	D
10·0	5·0	2·49	−1·57	2·45	−1·57	38	2·49	−1·57	51	D	D	D	D	D	D
10·0	8·0	7·45	−1·14	6·73	−1·20	135	7·38	−1·14	342	7·21	−1·40	20	D	D	D
20·0	1·0	0·27	−1·98	0·23	−1·97	57	0·26	−1·98	111	D	D	D	D	D	D
20·0	5·0	1·32	−1·98	1·27	−1·98	62	1·31	−1·98	86	D	D	D	D	D	D
20·0	10·0	2·49	−1·98	2·46	−1·98	47	2·49	−1·98	62	D	D	D	D	D	D
20·0	13·5	5·76	−1·89	5·40	−1·89	188	5·73	−1·89	367	D	D	D	D	D	D

Note: NS is the number of time steps for convergence and D means diverges

numerical and analytical predictions is quite satisfactory. To illustrate the need of establishing adequate time steps, a comparison between numerical results obtained with auto-adaptive time steps with the results obtained when time increments are arbitrarily chosen, is also shown. It can be seen that convergence, in the former cases, is not always guaranteed.

6.2. Example 2. Relative displacements of a joint family due to an applied loading from an initial state of stress

Some stress paths are simulated from an initial state of stress for the same joint family of Example 1. In each case a possible loading or unloading situation, in each or in both x and y directions, is considered. Table III shows the results for Barton–Bandis model:[2]

(1) The first column presents a scheme, which corresponds to the position of the initial, F_0, and the final, F_1, plastic surfaces. A value of the mobilized roughness coefficient, JRC_{mob}, interpreted as a hardening parameter related to the initial state of stress, corresponds to the initial surface. The final value of the roughness parameter corresponds to the final surface.
(2) The second column shows the values of tangential, u, and normal, v, displacements obtained analytically.
(3) The third column shows the results for the tangential and normal displacements given by program VISCO1. The value of the time increment is the least among the critical values of convergence and stability for both viscoplastic and viscoelastic idealizations obtained in each Gauss point. Tolerances TOL and TOL1 (equations (59) and (62)) are admitted to be equal to 10^{-3}.
(4) The fourth column presents the results for u and v obtained when the critical time step, defined by the program, is multiplied by a chosen factor, FAT equal to 100. These

Table III. Normal (v) and shear (u) displacements (in meters) for a single joint family, loaded from an initial state of stress with auto-adaptive time steps

Stress path σ_c, τ MPa		Analytical		Visco1 Minimum Δt TOL = TOL1 = 10^{-3}		Visco1 − FAT = 100 Minimum Δt TOL = TOL1 = 10^{-3}	
		$u \times 10^{-3}$	$v \times 10^{-4}$	$u \times 10^{-3}$	$v \times 10^{-4}$	$u \times 10^{-3}$	$v \times 10^{-4}$
1	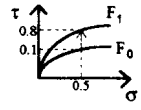	0·7030	1·6227	0·7020	1·6188	D	D
2	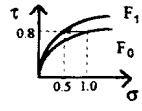	0·4004	0·8599	0·3996	0·8361	0·0000	0·1558
3	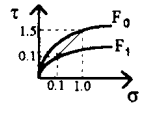	0·0000	0·2964	0·0000	0·2961	0·0000	0·2964
4	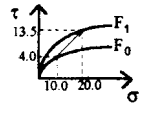	0·3719	−0·3428	0·3712	−0·3585	0·0000	−0·4080
5	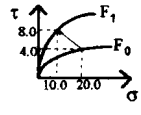	0·6393	0·7804	0·6366	0·7641	D	D
6	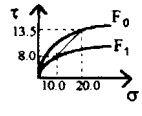	0·1691	0·4769	0·1678	0·4763	0·0000	0·4080

results serve only to demonstrate the need of defining an adequate time interval as it can be seen, in some examples, convergence may not be attained or the process converges to wrong values;

6.3. Example 3. Simplified analysis of a hypothetical dam foundation

This analysis has also been presented by Felipe.[14] In her work it was not always possible to establish a value for the time step which led to convergence. Then, the objective of this example is to verify the automatic and auto-adaptive definition of time steps for this case.

Figure 7 shows the geometry of the analysed problem. It corresponds to a concrete dam on a fractured rock foundation. Two sets of perpendicular joints are present in the foundation, one horizontal and another vertical, both with the same characteristics. An initial geostatic state of stress is considered and a value of 0·5 is admitted for the relation between horizontal and vertical

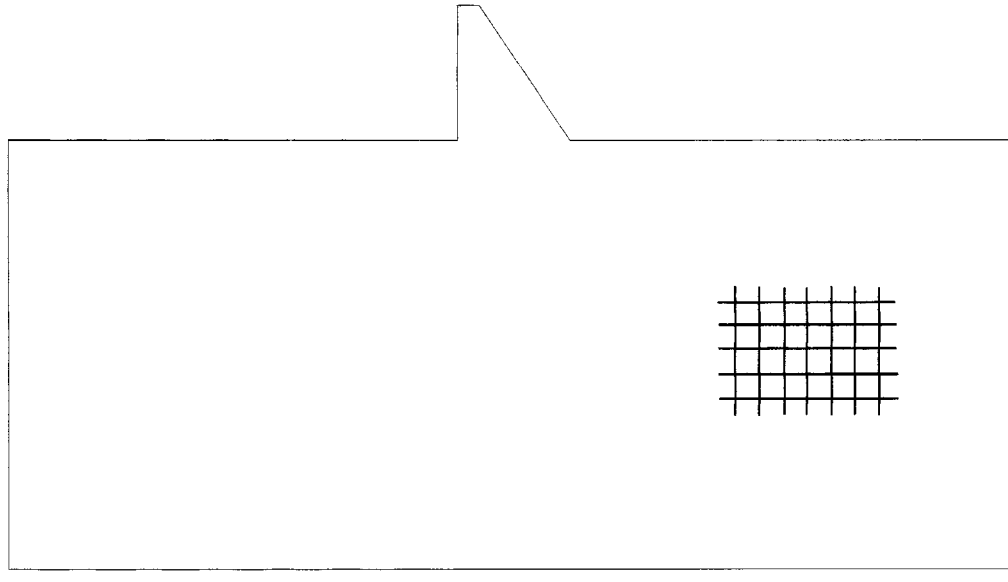

Figure 7. Geometry of the problem

stresses. The characteristics of the intact rock, the concrete and the joint families are summarized as follows:

Intact rock				Concrete		Joint families	
Depth (m)	0–30	30–70	70–190	E_c (MPa)	25 500	JRC	8·0
E_r (MPa)	10 000	20 000	25 000	υ_c	0·3	JCS (MPa)	80·0
υ_r	0·2	0·2	0·2	γ_c (MPa/m)	0·026	ϕ_r	32°
γ_{sub} (MPa/m)	0·017	0·017	0·017			s (m)	6·0
						e_0 (mm)	0·5

E_r, E_c—elasticity modulus of intact rock and of concrete, respectively.
υ_r, υ_c—Poisson coefficient of intact rock and of concrete, respectively
γ_{sub}—rock mass submerged specific weight
γ_c—concrete specific weight

Loading is applied according to the following scheme:

Stage	Loading
1	Dam construction
2	Filling up the reservoir

In loading stage 1, it is admitted that deformation of the foundation is caused only by dam weight. In stage 2, from the deformed configuration defined by stage 1, the water pressure is considered. It is admitted a total prescribed potential of 250 m upstream and 190 m downstream the dam.

The initial residual aperture, e_0, of both families was considered to be 0·5 mm. Coupled and uncoupled situations were analysed.

The structure is analysed in a plane strain situation. The final state of stress is a superposition of the initial geostatic state with the stress state defined by the analysis (coupled or uncoupled).

The finite element mesh, consisting of 16 elements and 67 nodes, is shown in Figure 8. The number of time steps necessary to reach a steady-state solution, in each stage of loading, is presented in Table IV.

Figures 9 and 10 show the distribution of total normal stresses (in MPa) in x direction for coupled and uncoupled flow, respectively. Figures 11 and 12 show the distribution of total normal stresses (in MPa) in y direction for coupled and uncoupled flow, respectively. Figures 13 and 14

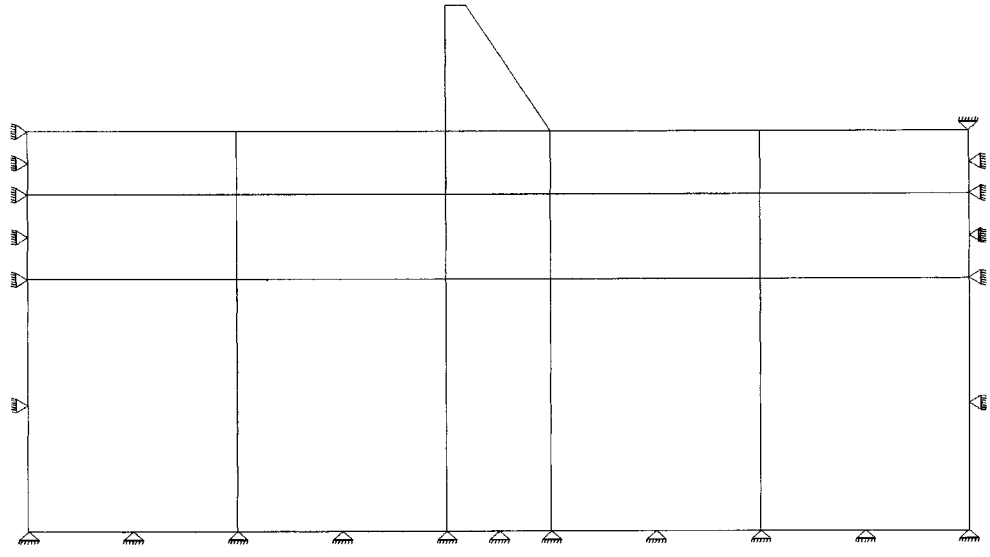

Figure 8. Finite element mesh

Table IV. Number of time steps for stationary solution

Flow	Number of time steps		
	Stage 1	Stage 2	Total
Coupled	76	1240	1315
Uncoupled	87	480	567

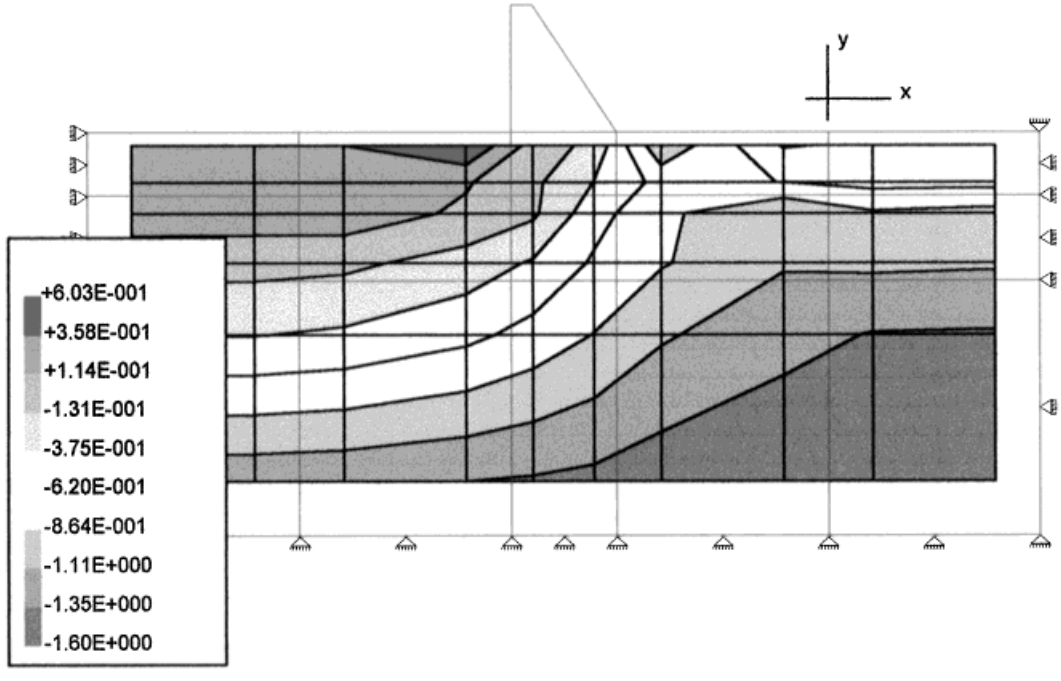

Figure 9. Normal stress distribution in x direction (MPa)—coupled flow

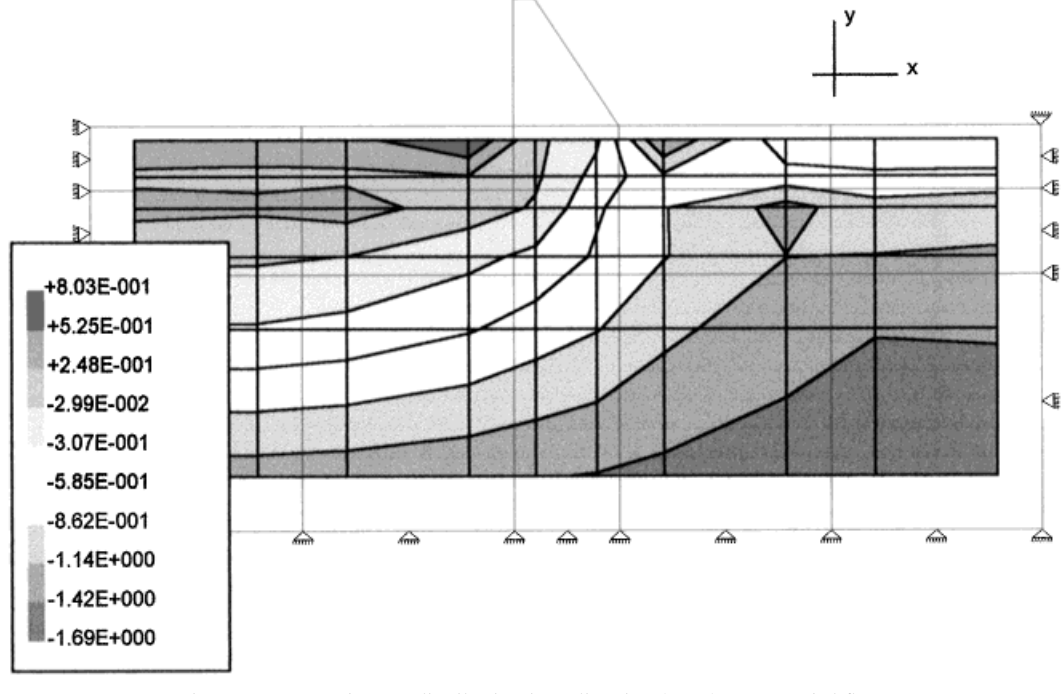

Figure 10. Normal stress distribution in x direction (MPa)—uncoupled flow

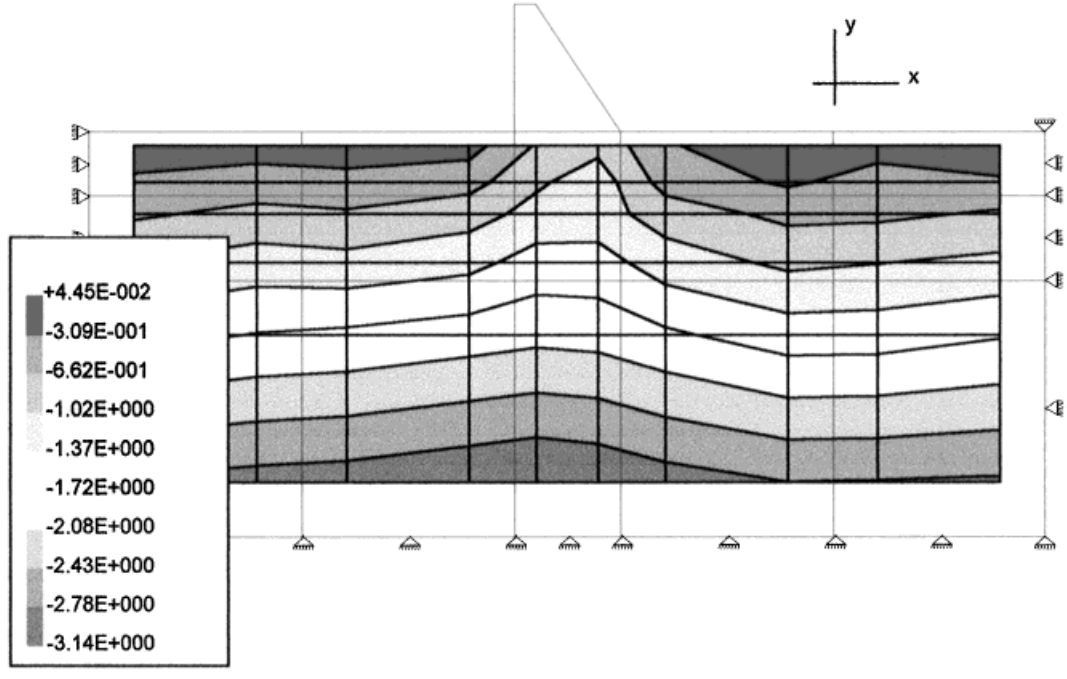

Figure 11. Normal stress distribution in y direction (MPa)—coupled flow

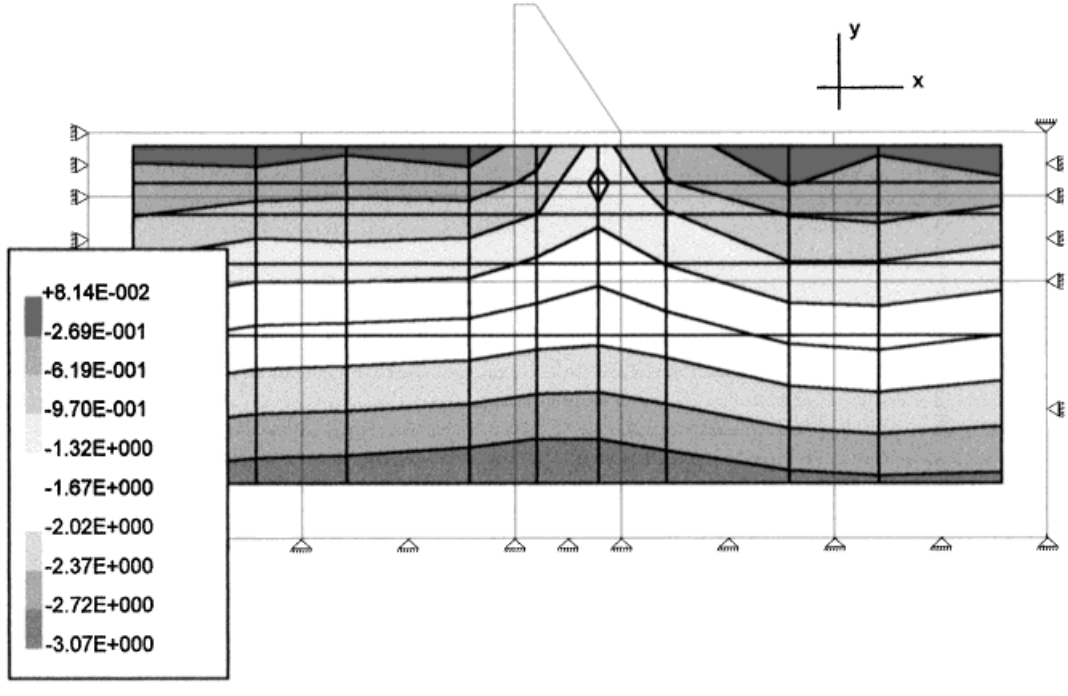

Figure 12. Normal stress distribution in y direction (MPa)—uncoupled flow

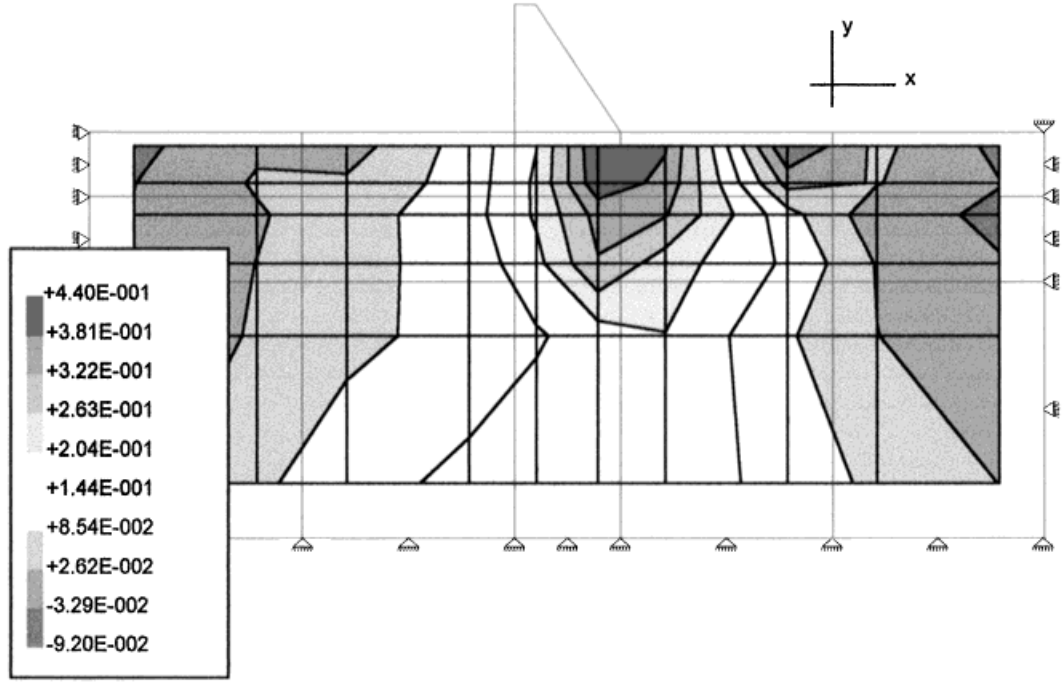

Figure 13. Shear stress distribution (MPa)—coupled flow

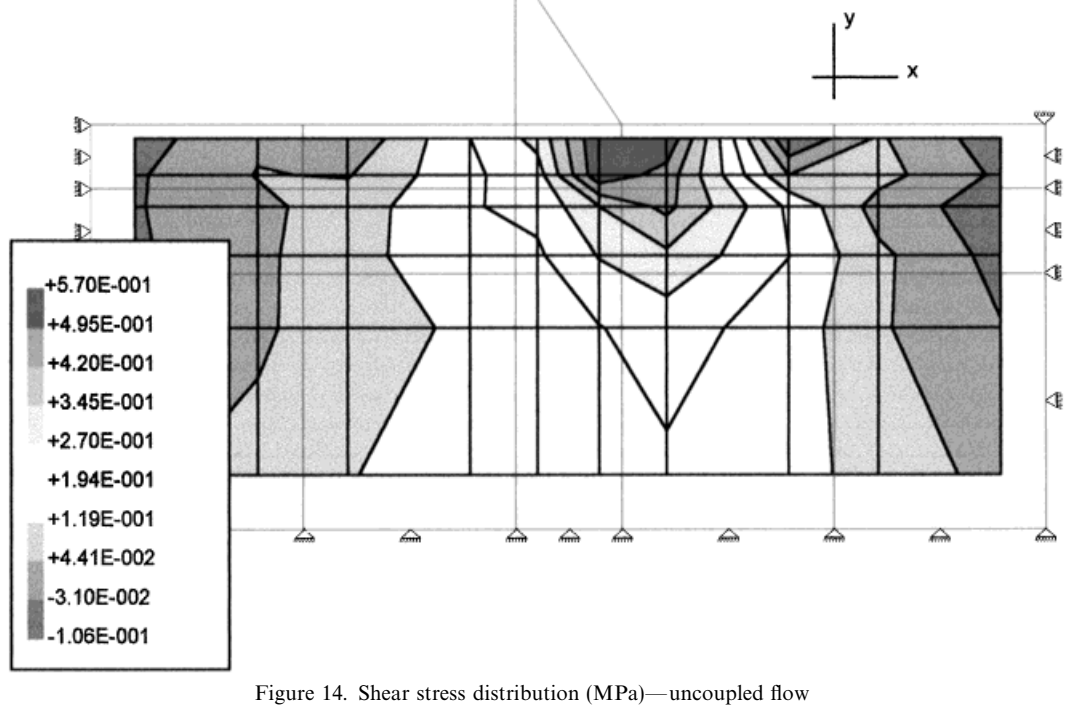

Figure 14. Shear stress distribution (MPa)—uncoupled flow

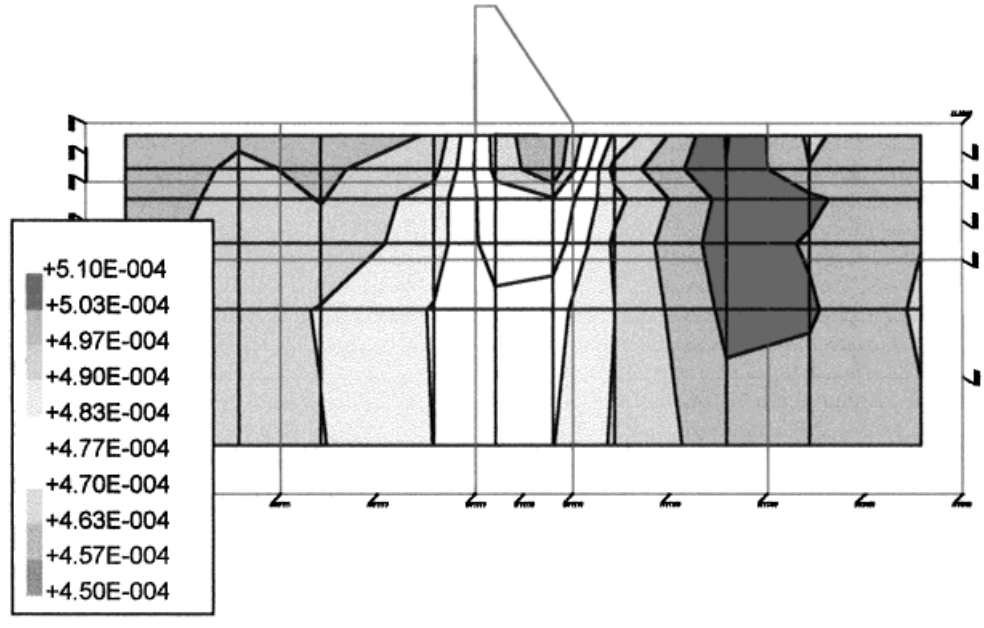

Figure 15. Horizontal joint aperture distribution (in meters)—coupled flow—initial aperture $e_0 = 0{\cdot}5$ mm

show the shear stress distributions (in MPa) for coupled and uncoupled flow, respectively. Horizontal and vertical joint aperture distributions (in millimeters) for coupled flow are shown in Figures 15 and 16, respectively (for uncoupled flow the horizontal and vertical aperture distributions remain unchanged). A comparison between total heads (in meters) in the cases of coupled and uncoupled flow is shown in Figures 17 and 18, respectively. The deformed configurations for both coupled and uncoupled flow are shown in Figures 19 and 20, respectively. Figures 21 and 22 show the values of self-adaptive time increments and the norm plotted against each step for both coupled and uncoupled analysis. As mentioned above, the consideration of an arbitrarily chosen time interval for this example has already been analysed[14] and convergence was not guaranteed. The automatic definition of self-adaptive time increments led to convergent and consistent results. A few conclusions are presented as follows:

(1) The consideration of coupling has a negligible influence in normal stress distributions (Figures 9–12). This occurs due to the low stress levels caused by the dam to the rock mass;
(2) The consideration of coupling, however, influenced significantly, the displacements. The coupled analysis generated greater displacements (Figure 19) than the uncoupled one (Figure 20), which is consistent with the fact that in the coupled analysis the initial joint apertures may vary;
(3) The total head distribution was modified in the coupled analysis (Figure 17), in the same way, qualitatively and quantitatively, observed by Felipe;[14]
(4) As observed by Erban,[27] in the case of coupled flow, after the filling up of the reservoir, the horizontal joint families under the dam are under compression with a corresponding reduction of the joint apertures (Figure 15). Consequently, the permeability of the rock mass in this direction is reduced. Due to water pressure upstream the dam, the vertical joint

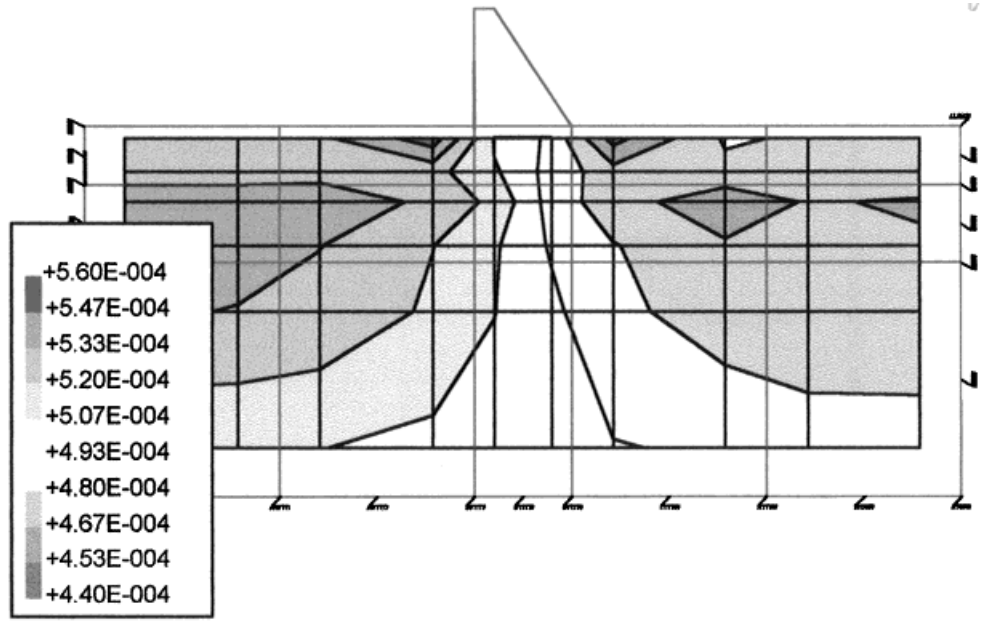

Figure 16. Vertical joint aperture distribution (in meters)—coupled flow—initial aperture $e_0 = 0{\cdot}5$ mm

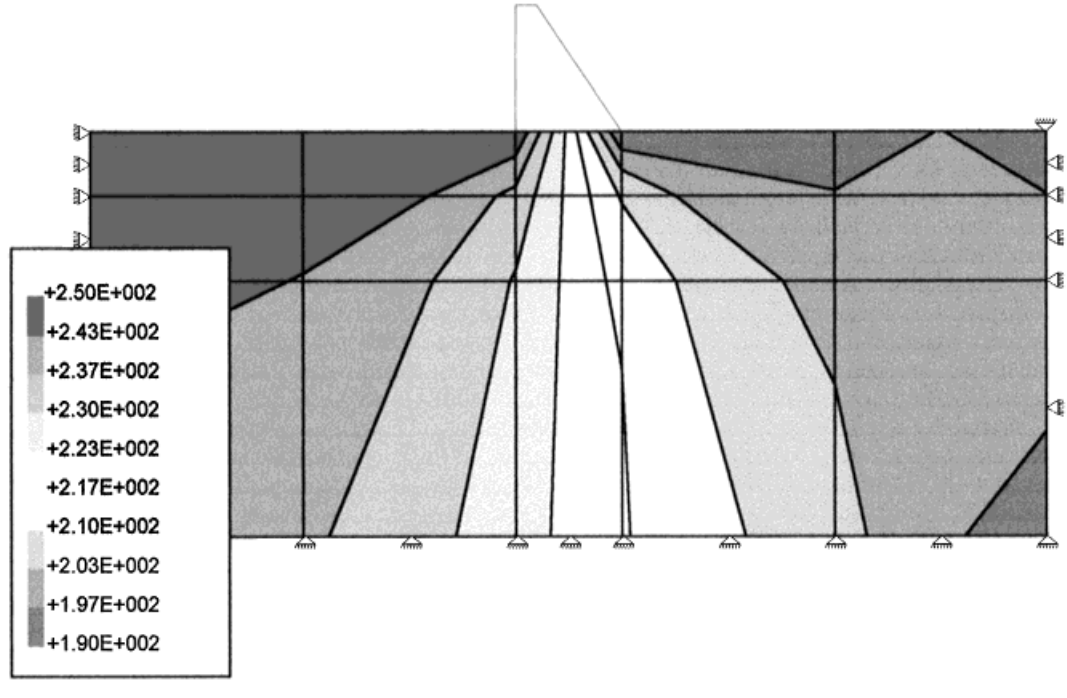

Figure 17. Total head (in meters)—coupled flow—initial aperture $e_0 = 0{\cdot}5$ mm

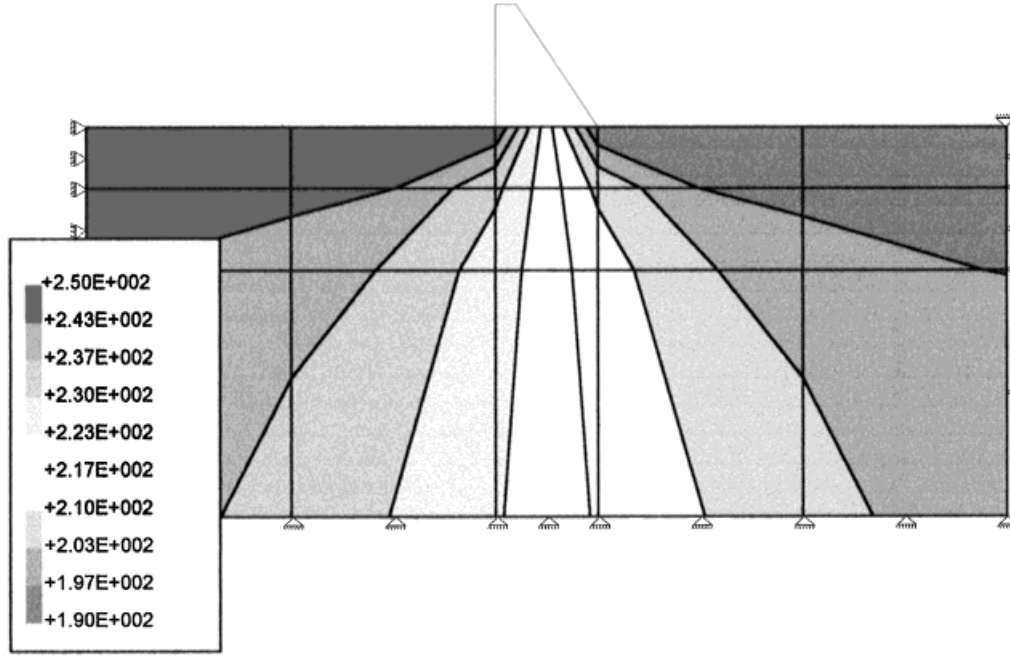

Figure 18. Total head (in meters)—uncoupled flow—initial aperture $e_0 = 0{\cdot}5$ mm

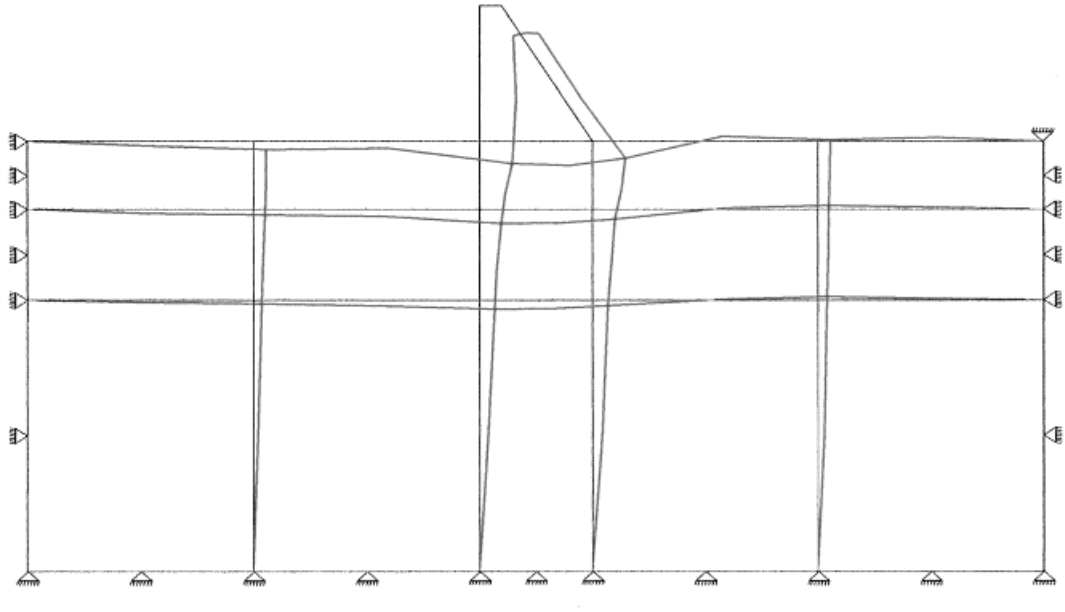

Figure 19. Deformed/undeformed configuration—coupled flow (displacements magnified by a factor of 2×10^3)

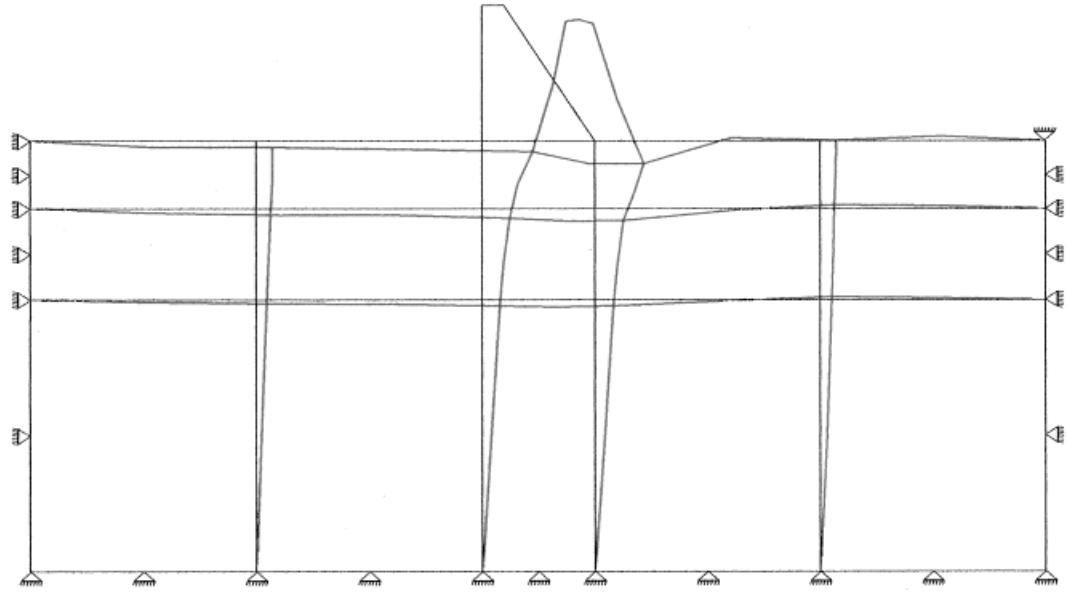

Figure 20. Deformed/undeformed configuration—uncoupled flow (displacements magnified by a factor of 2×10^3)

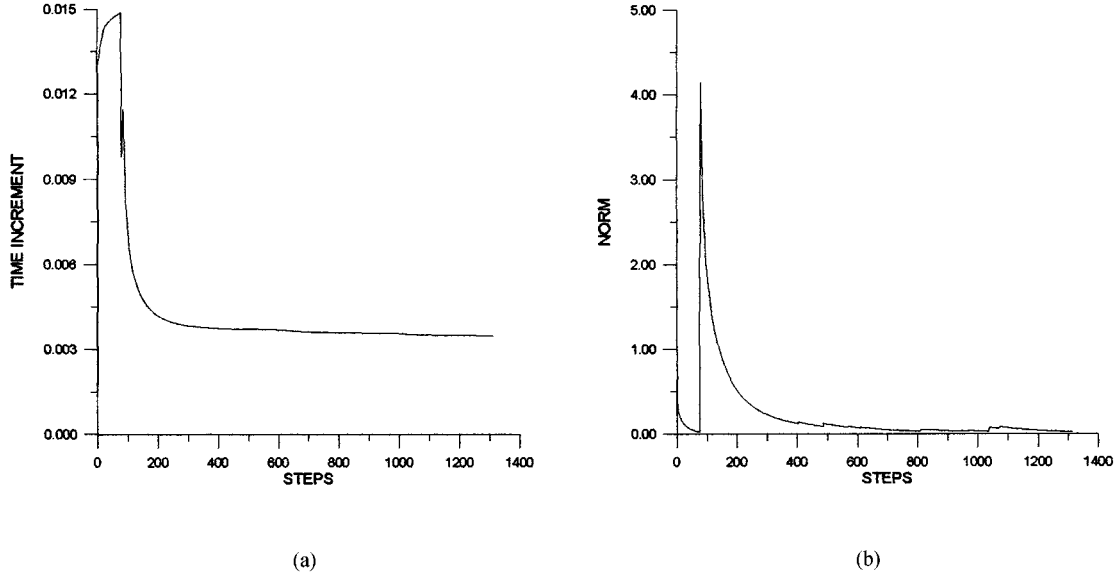

(a) (b)

Figure 21. Coupled flow: (a) self-adaptive time increments; (b) norm

families upstream open (Figure 16), increasing the permeability of the rock mass. Downstream, on the contrary, the vertical joint families tend to close occasioning a reduction in the permeability. As a consequence, it is observed a concentration of equipotential lines under the dam, which cause greater values of seepage forces in this region. These forces

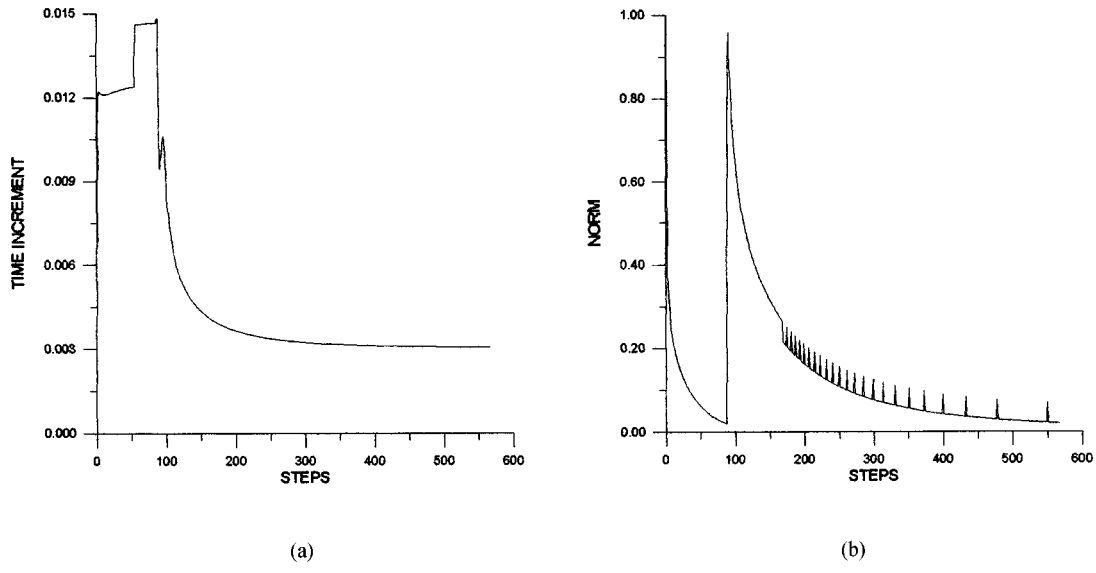

(a) (b)

Figure 22. Uncoupled flow: (a) self-adaptive time increments; (b) norm

cause, by their turn, an increase of permeability upstream and a reduction downstream originating new flow conditions.

Although not presented here, various other values of initial apertures for the joint families, as well as different finite element meshes, were analysed by program VISCO1 with time step control. In all cases convergent and consistent results were obtained. Again, for arbitrarily chosen time intervals, convergence was not guaranteed.

CONCLUSIONS

The main conclusion produced by this work is that the numerical implementation of the theoretical development for the automatic and auto-adaptive definition of the time increment used in the time integration process has worked successfully. It should be noted that the proposed theoretical development for the definition of critical time steps is generic and is, therefore, valid for any viscoplastic constitutive law.

Other examples, with closed-form solutions, were analysed[3] validating, this way, the automatic and self-adaptive calculation of time increments.

APPENDIX

Coefficients of matrix ψ_{i_ζ} *(equation (83a)) for B–B model*

$$F_\zeta = |\tau_\zeta| - \sigma_{c_\zeta} \operatorname{tg}\left(\mathrm{JRC}_{\mathrm{mob}_\zeta} \log\left(\frac{\mathrm{JCS}}{\sigma_{c_\zeta}}\right) + \phi_r\right)$$

$$\left(\frac{\partial Q}{\partial \sigma_c}\right)_\zeta = \mathrm{tg}\left(\frac{1}{M}\,\mathrm{JRC}_{\mathrm{mob}_\zeta}\log\left(\frac{\mathrm{JCS}}{\sigma_{c_\zeta}}\right)\right) \tag{109}$$

$$\left(\frac{\partial Q}{\partial \tau}\right)_\zeta = \pm 1$$

$$\psi_{11} = \bar{\gamma}_i\left[(-\mathrm{tg}\,A + C\sigma_{c_\zeta}\sec^2 A)\mathrm{tg}\,B - \left(F_\zeta\frac{C}{M}\sec^2 B\right)\right]_i$$

$$\psi_{12} = \bar{\gamma}_i[\mathrm{tg}\,B]_i \tag{110}$$

$$\psi_{21} = \bar{\gamma}_i\left[(-\mathrm{tg}\,A + C\sigma_{c_\zeta}\sec^2 A)\right]_i$$

$$\psi_{22} = \bar{\gamma}_i$$

where

$$A = \mathrm{JRC}_{\mathrm{mob}_\zeta}\log\left(\frac{\mathrm{JCS}}{\sigma_{c_\zeta}}\right) + \phi_r$$

$$B = \frac{1}{M}\,\mathrm{JRC}_{\mathrm{mob}_\zeta}\log\left(\frac{\mathrm{JCS}}{\sigma_{c_\zeta}}\right) \tag{111}$$

$$C = \mathrm{JRC}_{\mathrm{mob}_\zeta}\frac{\log(e)}{\sigma_{c_\zeta}}$$

REFERENCES

1. O. C. Zienkiewicz and G. N. Pande, 'Time dependent multilaminate model of rocks—A numerical study of deformation and failure of rock masses', *Int. J. Numer. Anal. Meth. Geomech.*, **1,** 219–247 (1977).
2. N. Barton, S. Bandis and K. Bakhtar, 'Strength deformation and conductivity of rock joints', *Int. J. Rock Mech. Min. Sci. Geomech.*, **22** (3)**,** 121–140 (1985).
3. I. C. Duarte, 'A numerical procedure for the analysis of the hydromechanical coupling in fractured rock masses', *Ph.D. Thesis* (in Portuguese), Catholic University, Rio de Janeiro, Brazil, 1994.
4. C.-F. Tsang, 'Coupled behaviour of rock joints', *Proc. Int. Symp. on Rock Joints*, Leon, Norway, 1990, pp. 505–518.
5. E. Vargas, 'Development and application of numerical models to simulate the behaviour of fractured rock masses', *Ph.D. Thesis*, University of London, 1982.
6. J. Lemos and L. Lorig, 'Hydromechanical modelling of jointed rock masses using the distinct element method', in *Mechanics of Jointed and Fractured Rock*, H. P. Rossmanith, (ed.), 1990, pp. 605–611.
7. J. Noorishad, M. Ayatolahi and P. Witherspoon, 'Coupled stress and fluid flow analysis of fractured rocks', *Int. J. Rocks. Mech. Min. Sci.*, **19,** 185–193 (1982).
8. T. Cho, B. Haimson and M. Plesha, 'Continuum modelling of porous rock with arbitrary point sets, including coupled deformation-diffusion behaviour', *7th Int. Conf. Rock Mechanics*, Aachen, 1991, pp. 805–881.
9. J. Kafritsas and H. Einstein, 'Coupled flow—deformation analysis of a dam foundation with distinct element method', *28th U.S. Symp. Rock Mech.*, Tucson, 1987, pp. 484–490.
10. A. E. Arruda, 'A method for the analysis of fractured rock masses based on the discrete block model', *M.Sc. Thesis* (in Protuguese), Catholic University, Rio de Janeiro, Brazil, 1989.
11. C. Wilson, 'An investigation of laminar flow in fractured porous media', *Ph.D. Thesis*, University of California, Berkeley, 1970.
12. N. Morgenstern and Guther, 'Seepage into an excavation in a medium possessing stress dependent permeability', *Proc. Symp. Percolation through Fissured Rock*, Stuttgart, 1972.
13. C. Erichsen, 'Gekoppelte spannungs-sickerstromungsberechungen von bauwerken in kluftigen fels uter berucksichtigung de nichlinearen spannungsverschiebungs-verhaltens von tremnflachen', Publ. no. 15 of Institut fur Felsmechanik/RWTH-Aachen, 1987.

14. S. Felipe, 'Numerical analysis of the hydromechanical behaviour of fractured rock masses', *M.Sc. Thesis* (in Portuguese), Catholic University, Rio de Janeiro, Brazil, 1992.
15. D. Owen and E. Hinton, *Finite Elements in Plasticity—Theory and Practice*, Pineridge Press Ltd., Swansea, U.K., 1986.
16. P. Perzyna, 'Fundamental problems in viscoplasticity', Adv. Appl. Mech., **9,** 243–377 (1966).
17. M. Rocha and F. O. Franciss, 'Permeability of rock masses determined from integral samples', in W. Hall (ed.), *Structural and Geotechnical Mechanics*, Prentice–Hall, Englewood Cliffs, NJ, 1977.
18. O. C. Zienkiewicz, *The Finite Element Method*, 3rd edn., McGraw-Hill, New York, 1977.
19. K. Bathe, *Finite Element Procedures in Engineering Analysis*, Prentice-Hall, Englewood Cliffs, NJ, 1982.
20. R. D. Cook, D. S. Malkus and M. E. Plesha, 3rd edn, *Concepts and Applications of Finite Element Analysis*, New York, 1989.
21. C. S. Desai and J. T. Christian, *Numerical Methods in Geotechnical Engineering*, McGraw-Hill, New York, 1977.
22. J. H. Argyris, L. E. Vaz and K. J. Willam, 'Improved solution methods for inelastic rate problems', *Comput. Meth. Appl. Mech. Engng*., **16,** 231–277 (1978).
23. I. Cormeau, 'Numerical stability in quasi-static elasto/visco-plasticity', *Int. J. Numer. Meth. Engng*., **9,** 109–127 (1975).
24. L. G. Araújo, 'Finite element viscoplastic analysis of fractured rock masses', *M.Sc. Thesis* (in Protuguese), Catholic University, Rio de Janeiro, Brazil, 1989.
25. S. Felipe, E. Vargas; L. E. Vaz and I. Duarte, 'An implementation for the numerical analysis of the hydromechanical coupling in fractured rock masses', *Proc. of the 1st Int. Workshop on Appl. of Comp. Mechs. in Geotech. Engineering*, Rio de Janeiro, Brazil, 1991, pp. 29–31.
26. E. Vargas, S. Felipe, L. E. Vaz, I. Duarte and L. R. Sousa, 'A continuum analysis of the hydromechanical coupling in fractured rock masses', *Fractured and Jointed Rock Masses Conf*., Lake Tahoe, California, E.U.A, Balkema, 1992, pp. 587–593.
27. P.-J. Erban and K. Gell, 'Consideration of the interaction between dam and bedrock in a coupled mechanic-hydraulic FE-program', *Rock Mech. Rock Engng*, **21,** 99–117 (1988).

